

A TRIDENT SCHOLAR PROJECT REPORT

NO. 189

"Picosecond Optical Mixing in Photorefractive Materials"

AD-A256 824



DTIC
LECTE
NOV 12 1992
B D

UNITED STATES NAVAL ACADEMY
ANNAPOLIS, MARYLAND

This document has been approved for public
release and sale; its distribution is unlimited.

92-29345

U.S.N.A. - Trident Scholar project report; no. 189 (1992)

"Picosecond Optical Mixing in Photorefractive Materials"

A Trident Scholar Project Report

by

Midshipman C. Andrew McCartney, Class of 1992

U. S. Naval Academy

Annapolis, Maryland

Steven R. Montgomery

**Adviser: Assistant Professor, Steven R. Montgomery
Physics Department**

Accepted for Trident Scholar Committee

Francis D. Correll

Chair

8 May 1992

Date

USNA-1531-2

REPORT DOCUMENTATION PAGE

Form Approved
OMB No. 0704-0188

Public reporting burden for this collection of information is estimated to average 1 hour per response, including the time for reviewing instructions, searching existing data sources, gathering and maintaining the data needed, and completing and reviewing the collection of information. Send comments regarding this burden estimate or any other aspect of this collection of information, including suggestions for reducing this burden, to Washington Headquarters Services, Directorate for Information Operations and Reports, 1215 Jefferson Davis Highway, Suite 1204, Arlington, VA 22202-4302, and to the Office of Management and Budget, Paperwork Reduction Project (0704-0188), Washington, DC 20503.

1. AGENCY USE ONLY (Leave blank)		2. REPORT DATE 8 May 1992	3. REPORT TYPE AND DATES COVERED Final 1991/92	
4. TITLE AND SUBTITLE PICOSECOND OPTICAL MIXING IN PHOTOREFRACTIVE MATERIALS			5. FUNDING NUMBERS	
6. AUTHOR(S) McCartney, C. Andrew				
7. PERFORMING ORGANIZATION NAME(S) AND ADDRESS(ES) U.S. Naval Academy, Annapolis, Md.			8. PERFORMING ORGANIZATION REPORT NUMBER U.S.N.A. - TSPR; 189 (1992)	
9. SPONSORING/MONITORING AGENCY NAME(S) AND ADDRESS(ES)			10. SPONSORING/MONITORING AGENCY REPORT NUMBER	
11. SUPPLEMENTARY NOTES Accepted by the U.S. Trident Scholar Committee				
12a. DISTRIBUTION/AVAILABILITY STATEMENT This document has been approved for public release; its distribution is UNLIMITED.			12b. DISTRIBUTION CODE	
13. ABSTRACT (Maximum 200 words) The interaction of laser light in a photorefractive crystal can form a grating that holds promise as a future means of information storage and optical processing. The goal of the project was to examine grating formation when the laser light consists of pulses of a few picoseconds duration and make a comparison with continuous wave laser light. Toward this end, a device called an optical autocorrelator was constructed to measure the duration of the ultrashort pulses, as they are too brief to be measured by conventional electronic means. Two measurable consequences of the photorefractive effect were examined: beam fanning and self-pumped phase conjugation. Significant differences between pulsed and continuous wave input were noted, and insight into self-pumped phase conjugation was gained. The results indicate the response of photorefractive crystals to ultrashort laser pulses remains an attractive item of study.				
14. SUBJECT TERMS LASER BEAMS: PHOTOREFRACTIVE MATERIALS			15. NUMBER OF PAGES 58	
			16. PRICE CODE	
17. SECURITY CLASSIFICATION OF REPORT UNCLASSIFIED	18. SECURITY CLASSIFICATION OF THIS PAGE UNCLASSIFIED	19. SECURITY CLASSIFICATION OF ABSTRACT UNCLASSIFIED	20. LIMITATION OF ABSTRACT	

Abstract

The interaction of laser light in a photorefractive crystal can form a grating that holds promise as a future means of information storage and optical processing. The goal of the project was to examine grating formation when the laser light consists of pulses of a few picoseconds duration and make a comparison with continuous wave laser light. Toward this end, a device called an optical autocorrelator was constructed to measure the duration of the ultrashort pulses, as they are too brief to be measured by conventional electronic means.

Two measurable consequences of the photorefractive effect were examined: beam fanning and self-pumped phase conjugation. The grating formation time and grating strength were compared in the beam fanning case, while the reflectivity, signal characteristics and incidence angles were also included in the self-pumping comparison. Significant differences between pulsed and continuous wave input were noted, and insight into self-pumped phase conjugation was gained. The results indicate the response of photorefractive crystals to ultrashort laser pulses remains an attractive item of study.

DTIC QUALITY INSPECTED 4

Accession For	
NTIS GRA&I	<input checked="" type="checkbox"/>
DTIC TAB	<input type="checkbox"/>
Unannounced	<input type="checkbox"/>
Justification	
By _____	
Distribution/	
Availability Codes	
Dist	Avail and/or Special
A-1	

Table of Contents

1. Introduction to the Photorefractive Effect	4
1.1) History	4
1.2) Uses	4
1.3) Project Objectives	5
2. Autocorrelation	6
2.1) Necessity of Autocorrelating	6
2.2) General Autocorrelation Principles	6
2.3) Second Harmonic Signals	8
2.4) Autocorrelator Output Signal	11
2.5) Autocorrelation Function	13
2.6) Parallel Mirror Autocorrelator	14
2.7) Autocorrelator Construction and Results	15
3. Basic Principles of the Photorefractive Effect	17
4. Properties of Photorefractive Materials	20

5. Measurable Consequences of the Photorefractive Effect	22
5.1) Beam Fanning	22
5.2). Optical Phase Conjugation	23
5.2.a. Holography	25
5.3.b. Four-Wave Mixing	26
5.4.c. Self-Pumped Phase Conjugation	27
6. Experimental Set-up	30
6.1) Picosecond Laser System	30
6.2) Beam Fanning	31
6.3) Self-Pumped Phase Conjugation	45
7. Conclusions and New Directions	55
8. References	57
Appendix A: Equipment List	58

1. Introduction to the Photorefractive Effect

1.1) History. As recently as 25 years ago, photorefractive properties were seen as a bothersome intrusion that thwarted the potential usefulness of many optical materials. Scientists at Bell Laboratories were testing crystals for potential use as second-harmonic generators by directing laser light into them, when they observed that after a short period of time the incident beam no longer passed directly through the crystal but was increasingly scattered. Thus began the study of a new area of non-linear optics, the photorefractive effect, that is still not completely understood.¹ Light passing through a photorefractive crystal semipermanently alters the crystal's optical properties, producing changes that vary in duration from seconds to years, depending on the material.

1.2) Uses. Potential applications for photorefractive materials include holographic memory storage, the optical analog of a transistor, phase conjugate mirrors, coherent optical excisors, as well as components for optical computers that would be able to process information at much faster rates than the electronic means available today.¹

1.3) Project Objectives. Most studies of the photorefractive effect have been made using continuous wave laser sources. The objective of this project was to investigate differences between the response of a photorefractive material to continuous wave sources and the response using ultrashort laser pulses. Toward that end, the first part of the project required the construction of a device for measuring the duration of the ultrashort laser pulses, called an optical autocorrelator. The two effects of the photorefractive materials that we examined were beam fanning and self-pumped phase conjugation.

2. Autocorrelation

2.1) Necessity of Autocorrelating. The ability to produce temporally short optical pulses, such as the ultrashort pulses of this experiment, has outstripped the means to detect them using conventional electronics. Fast photodiodes can be used to detect temporal intensity profiles for pulses as short as one hundred picoseconds, and streak cameras can detect the temporal intensity profiles of pulses of slightly less than five picoseconds^{2,3}. Though these are presently the best methods to obtain detailed information about the temporal intensity profiles of short optical pulses, the pulses used for this experiment were shorter than the five picosecond limit of streak cameras, and an optical autocorrelator was constructed to approximate the pulse duration of the ultrashort laser pulses.⁴

2.2) General Autocorrelation Principles. The optical autocorrelator consists of two parts. The first part splits an optical pulse train and provides relative delay between the resulting pulse trains before sending them to the second part of the system, a nonlinear medium and detector that is sensitive to pulse overlap. Usually, the splitting and delay portion consists of a Michelson interferometer (the design used in this experiment) with one leg fixed in length while the other leg has a time varying path length, as shown in Figure 1.

The Autocorrelator

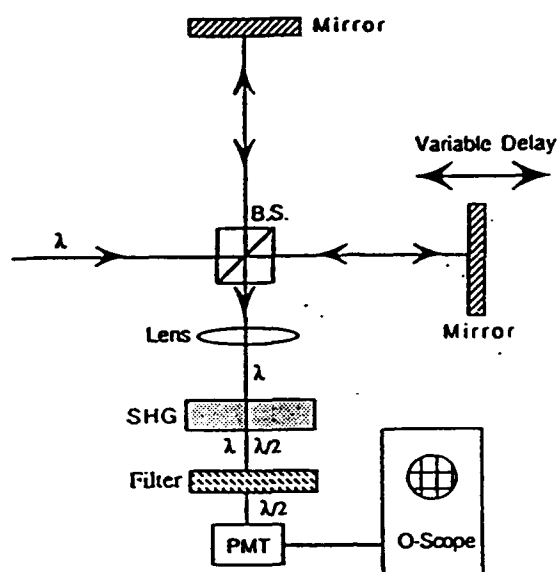
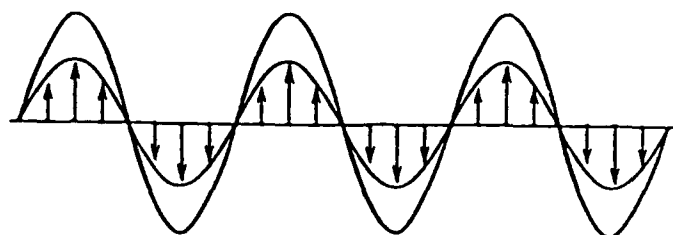


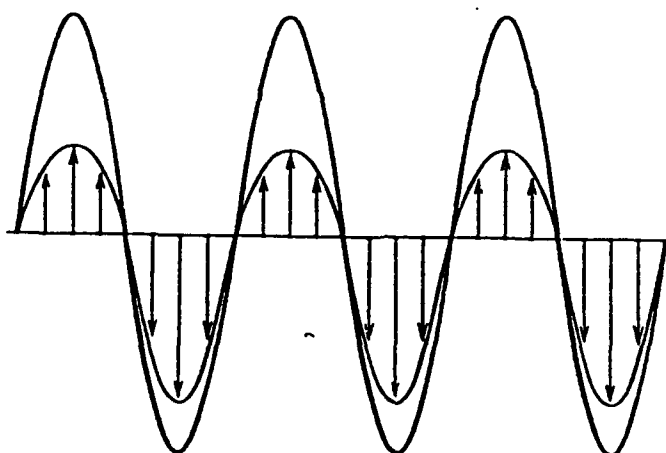
Figure 1.

The nonlinear medium consists of a second harmonic crystal followed by a filter for blocking the input light of wavelength λ and a photomultiplier tube, also shown in Figure 1, for detecting the second harmonic light and thus pulse overlap. The relative delay between the pulse trains then proceeds at a rate determined by the rate of path length increase in the variable leg of the interferometer. This rate can be slow enough that the overlap signal is easily detectable by a conventional oscilloscope. If the rate of path length increase is known then a measurement of overlap duration from the scope gives an estimate of the pulse duration.

2.3) Second Harmonic Signals. Second harmonic generating crystals are birefringent, non-centrosymmetric, and optically non-linear materials that respond to incident light so that a non-symmetric polarization wave is formed⁵, as shown in Figure 2.



Symmetric Polarization Wave
(Centrosymmetric Materials)



Non-Symmetric Polarization Wave
(Non-Centrosymmetric Materials)

Figure 2. Polarization Wave Comparison from Reference 5

The non-symmetric polarization wave is the sum of three components: fundamental polarization, second harmonic polarization, and steady d.c. polarization⁵, as shown in Figure 3.

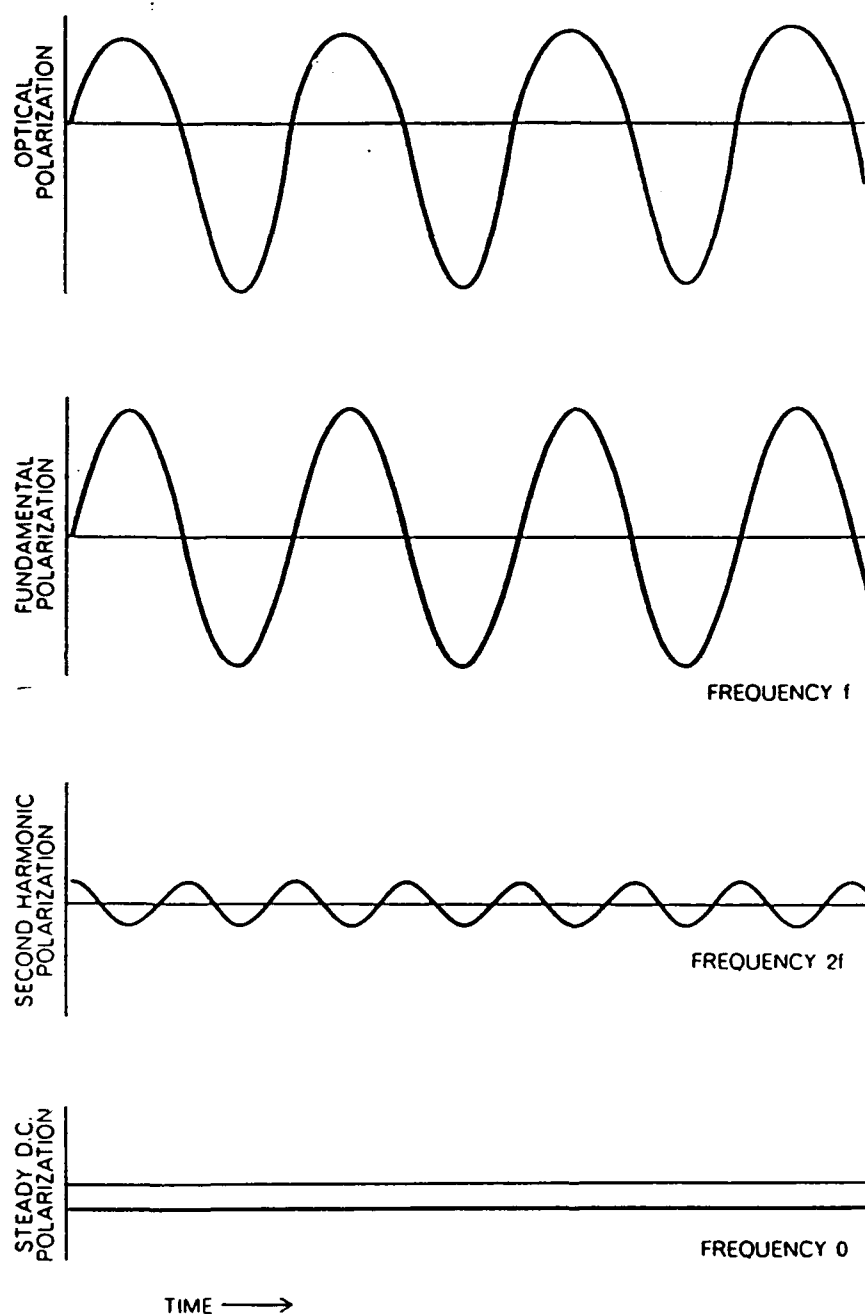


Figure 3. Non-Symmetric Polarization Wave Components
from Reference 5

The second harmonic component can be separated from the fundamental component using an ultraviolet transmitting filter. The d.c. component does not propagate.

The propagation direction of the input light must be at an angle that matches the velocities between the ordinary (fundamental) and extraordinary (second harmonic) polarizations in the material⁵, as shown in Figure 4.

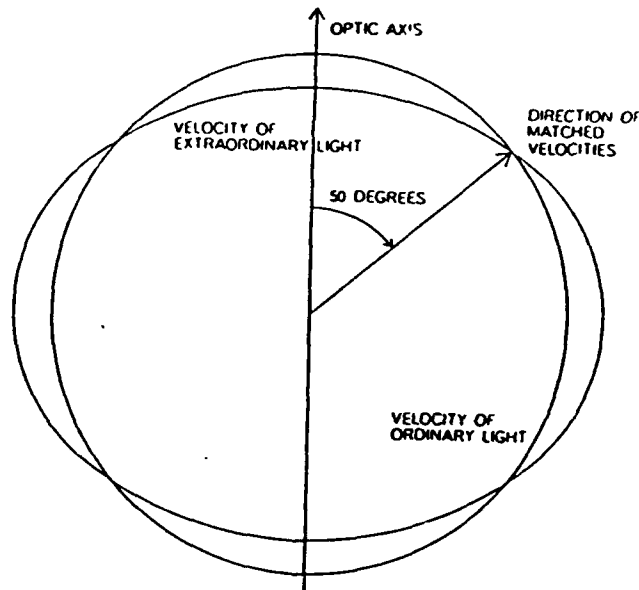


Figure 4. Propagation Speed of Extraordinary and Ordinary Polarization States with Respect to Angle of Travel in the Material from Reference 5

If both polarization states travel at the same speed throughout the crystal, then the second harmonic signal generated at different depths into the crystal will constructively interfere with that produced elsewhere in the crystal.

The component of the original frequency can then be filtered out after the light exits the crystal. The resulting pulse trains that

emerge from the filter are composed of second harmonic waves and made incident onto a photomultiplier for detection.

2.4) Autocorrelator Output Signal. The autocorrelation signal is a result of the overlap between the two pulse trains and is shown in Figure 5, and follows from the relationship of the intensities of the signals and their behavior when the delay is varied linearly. The intensity of a second harmonic ($I_{2\omega}$) is proportional to the square of the intensity of the fundamental (I_{ω})^{6,7}:

$$I_{2\omega} \propto I_{\omega}^2 \quad (1)$$

The intensity leaving the Michelson interferometer is the sum of the intensities from the two legs such that

$$I_T = I_1 + I_2 \quad (2)$$

The second harmonic signal intensity is proportional to I_T^2 as

$$I_{2\omega} \propto I_1^2 + I_2^2 + 2(I_1 I_2) \quad (3)$$

Since our detector is too slow to detect the pulses, as stated before, the output at our detector will be the time average of the second harmonic signal, as follows:

$$\text{Detected Output} \propto \langle I_1^2 \rangle + \langle I_2^2 \rangle + 2\langle I_1 I_2 \rangle \quad (4)$$

Since the input from the two legs is identical except for a time delay, we can equate them as follows:

$$I_2(t) = I_1(t + \tau) \quad (5)$$

Substituting this relationship in the equation (4) yields:

$$\text{Detected Output} \propto \langle I_1^2(t) \rangle + \langle I_1^2(t + \tau) \rangle + 2\langle I_1(t)I_1(t + \tau) \rangle \quad (6)$$

Dropping the subscript and using the fact that

$$\langle I_1(t) \rangle = \langle I_1(t + \tau) \rangle, \quad (7)$$

equation (6) becomes

$$\text{Detected Output} \propto 2\langle I^2(t) \rangle + 2\langle I(t)I(t + \tau) \rangle \quad (8)$$

This proportionality can also be written in the form

$$\text{Detected Output} \propto 1 + \frac{\langle I(t)I(t + \tau) \rangle}{\langle I^2(t) \rangle} \quad (9)$$

where the constant term corresponds to a constant baseline portion of the output that is insensitive to the delay, while the second term is dependent on the delay. The second term is a measure of pulse overlap and varies between zero and one. When the second term is zero (no overlap) the detected output is just the baseline signal.

When the second term reaches its peak value of one, the signal is twice the magnitude of the baseline value. Thus, we see a 2:1 ratio between the peak and baseline outputs, as shown in Figure 5. The spike in the center of the signal results as the overlapping pulses are coherent. When coherent, the fields of the overlapping pulses are added, rather than their intensities, producing a coherence spike with a 3:1 ratio.⁸

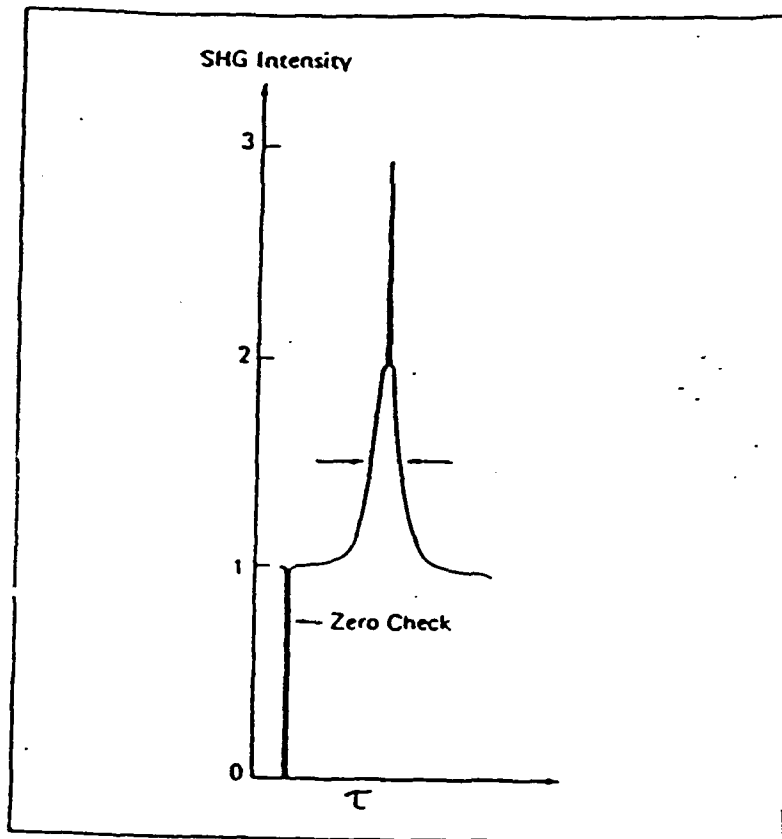


Figure 5. Autocorrelator Output Signal

2.5) Autocorrelation Function. The numerator of the overlap term is called the second order autocorrelation of $I(t)$, and is written in explicit integral form as

$$\langle I(t)I(t + \tau) \rangle = G(\tau) = \int_{-\infty}^{\infty} I(t)I(t + \tau) dt \quad (10)$$

Letting $\tau = 0$ be defined as perfect overlap of the pulses from each leg of the autocorrelator, equation (10) shows the shape of the signal as a symmetric function of delay. By assuming the functional form

of $I(t)$, an approximate value of the time duration of the pulse, t_p , can be determined from $G(t)$. It is shown in Reference 4 that from the Fourier transform of $G(\tau)$, $I(t)$ can not be extracted from $G(\tau)$ alone, except in the case of a symmetric pulse profile. Thus, an assumption of $I(t)$ is necessary to determine t_p .⁴

2.6) Parallel Mirror Autocorrelator. In this experiment, the varying path length was set up using a system of rotating parallel mirrors, as outlined in reference 9 and shown in Figure 6.

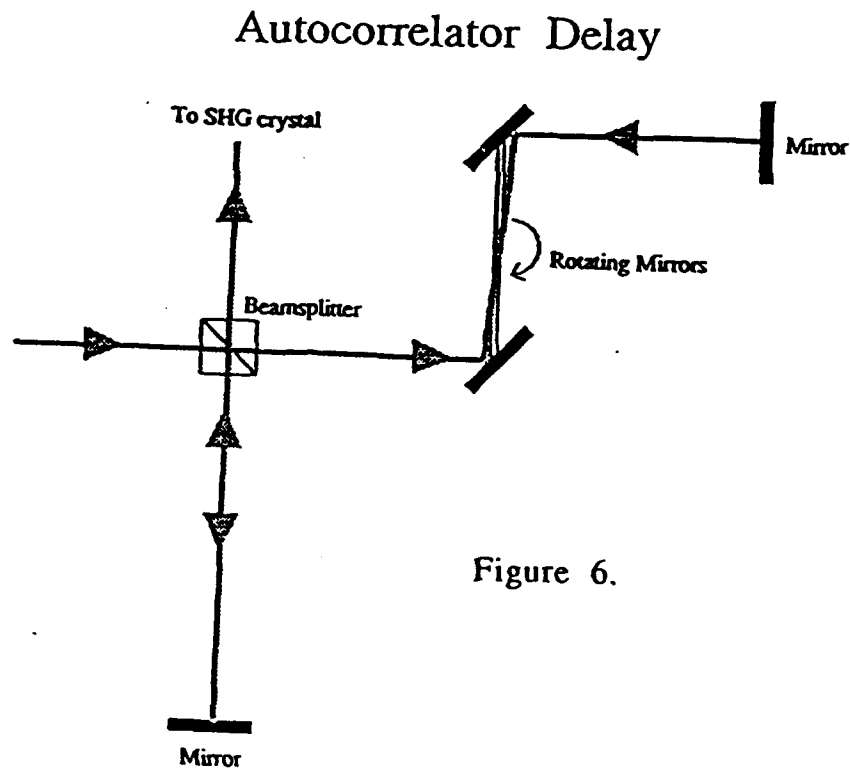


Figure 6.

There are several advantages to this system of autocorrelation over others. The mirrors rotate at a constant frequency and produce a train of pulses whose delay varies linearly with time, with respect to the train of pulses from the fixed leg.⁹ The medium between the mirrors (air) is virtually non-dispersive, preserving the shape of the pulses in the delayed leg.⁹ Also, the system is virtually insensitive to vibration because external vibrations affect both mirrors equally.⁹ These advantages, and the continuous rotation of the mirrors, produce a stable autocorrelation signal that can be monitored on an oscilloscope and used to aid in the tuning and stabilization of the laser system.

2.7) Autocorrelator Construction and Results. For the autocorrelator constructed in this project, the rotating parallel mirrors of the Femtochrome Research Corporation, Model FR-203 variable delay generator were used. The unit was modified by removing extraneous mirrors that did not serve any purpose here. The radius of the rotating arm in this unit is about three inches while the rotation rate is about 5 Hz.

The second harmonic generator, a 1 mm x 5 mm x 5 mm crystal of beta barium borate (BBO), was purchased from Inrad Corporation. This crystal was chosen since it has a wide range of operating wavelengths (450 to 850 nm) that more than covers the entire wavelength range of the dye laser.

For detection of the second harmonic signal a Hamamatsu photomultiplier tube was used in conjunction with a Hoya optics uv transmitting filter. The high voltage supplied to the photomultiplier

tube ranged between 300 volts and 600 volts, depending on the average power of the input pulse train which varied from a few to more than a hundred milliwatts of optical power.

The signals obtained corresponded very favorably to the classic signal shown in Figure 5. There was very little noise when the system was optimally tuned, a state that was in fact impossible before the completion of the autocorrelator since noise on the dye laser beam does not significantly effect the average output power of

From the calibration equation given in Reference 9, the delay rate was determined to be 33 picoseconds per millisecond. This value was checked by mounting the fixed mirror on a micrometer driven translator and comparing the time shift of the signal on the oscilloscope to the translation distance of the "fixed" mirror. The delay was once again found to be 33 picoseconds per millisecond.

The range of pulse lengths measured varied from 2.6 picoseconds to 13 picoseconds, the latter obtained by placing microscope cover slips in the dye laser cavity to act as an etalon. An etalon restricts the bandpass of the dye laser to produce a longer transform limited pulse.

3. Basic Principles of the Photorefractive Effect

When light is incident on a photorefractive crystal interference maxima and minima can be set up in the material due to the interference of overlapping coherent beams.^{1,10} In a photorefractive material mobile charges, either positive holes or negative electrons, depending on the material, slowly diffuse away from the maxima and collect in the minima. As mobile charges build up in the interference minima, the opposite charge is left in the maxima inducing an electric field between the maxima and minima that can become strong enough to alter the refractive index of the material via a lattice distortion known as the linear electrooptic effect.^{10,11} This semipermanent change occurs wherever bright and dark regions exist in the crystal and can remain in the crystal even after the light is removed, if it is a poor conductor in the dark.¹ Two beams of light, as from a laser and signified by A_1 and A_2 in Figure 7, form an interference pattern that is oscillatory in nature. This pattern, inside a photorefractive crystal, results in distribution of charges and crystal lattice distortions that are oscillatory in nature. The refractive index has thus been altered periodically and with the same spatial frequency as the initial interference pattern, but one quarter of a period out of phase with respect to the varying light intensity, as shown in Figure 7.^{1,6,10}

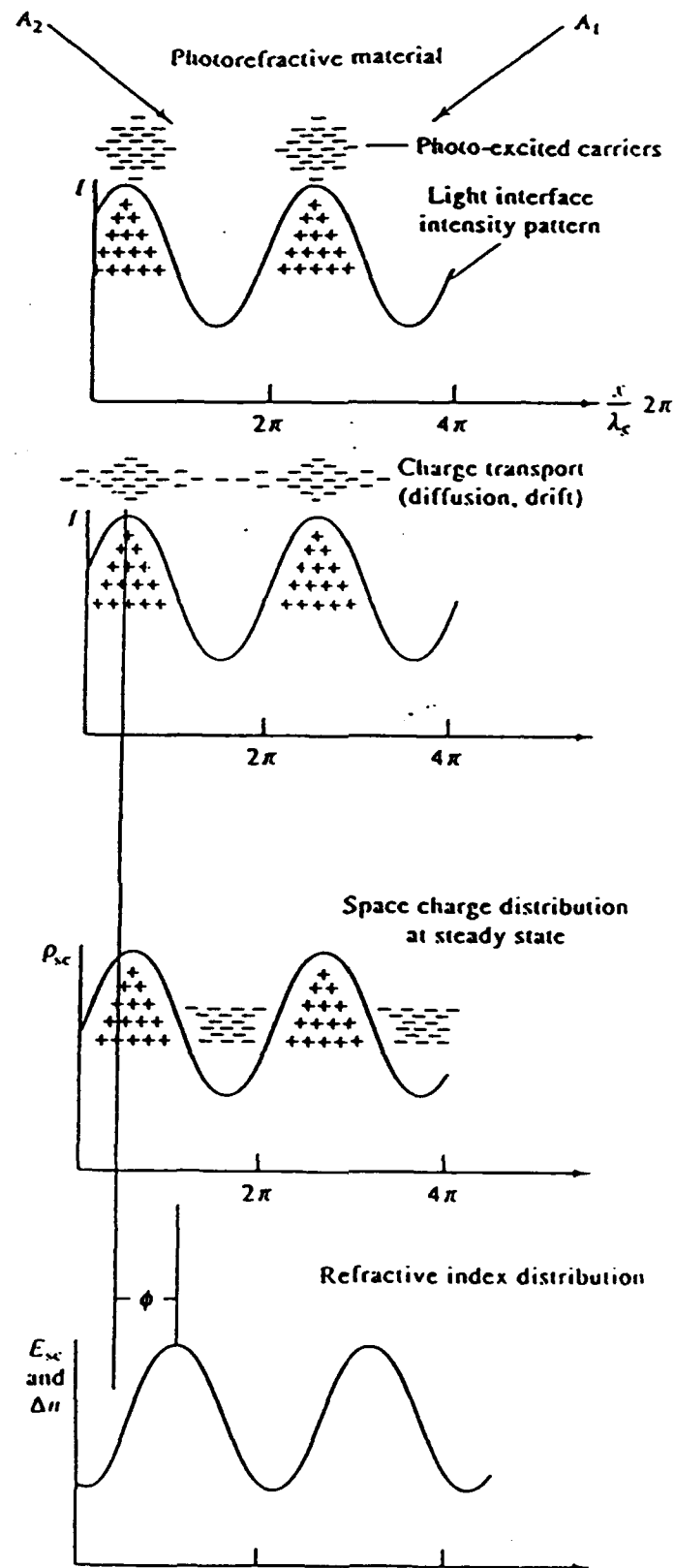


Figure 7. Photorefractive Process (top to bottom) from Reference 6

The refractive index variation is called a grating since it is able to scatter light in a manner similar to a diffraction grating and it is said to be "written" in the material. The sign of the mobile charge carrier (negative electrons or positive holes) determines the direction of the relative phase shift between the interference pattern and the refractive index grating. The phase shift of the grating has the effect of scattering light to only one side of the transmitted beam. It is the direction of this relative phase shift that determines the side to which the incident beam is "diffracted." The parameters of greatest interest when evaluating the gratings of photorefractive materials are the scattering efficiency of the gratings, formation times of the gratings, and the duration of the gratings in the dark.

4. Characteristic Properties of Photorefractive Materials

The photorefractive effect is a result of many properties of photorefractive materials. Photorefractive materials are non-centrosymmetric, i.e., they do not possess inversion symmetry about any given point, a requirement imposed by the linear electrooptic effect. This property is most easily explained by looking at its opposite, a centrosymmetric material. In a unit cell of a centrosymmetric material, observation of the crystal at any point, \vec{r} , in comparison to the one at $-\vec{r}$ (\vec{r} being the position vector relative to the given point) yields no difference in the structure or properties.⁶ However, in non-centrosymmetric materials, differences do exist between the two opposite translations.

The crystal used in this study of the photorefractive effect relies on the alignment of ferroelectric domains instead of an externally applied field. In a ferroelectric crystal, small domains exist that each have an electric dipole. If, by the application of heat, pressure or electric field, the domains can be aligned, then the crystal is said to be poled. Poled crystals have their centrosymmetric symmetry broken by the resulting dipole field and do not require an external field for observing the photorefractive effect.

Photorefractive crystals can be produced synthetically to have the above properties, and the ability to produce high-quality crystals is constantly improving. Impurities are often intentionally introduced into the crystals, to enhance the photorefractive effect.

The crystals are very expensive to produce and thus are presently only used for experimental purposes in small-scale laboratory environments.¹⁰

Photorefractive effects have been studied in many materials including transparent crystals, semiconductors, piezoelectric ceramics and more recently, polymers. The photorefractive material used for this study was a 5 mm x 5 mm x 5 mm crystal of cerium doped barium strontium potassium sodium niobate (BSKNN), a member of the tungsten-bronze family of crystals that has tetragonal structure. BSKNN crystals have been previously shown to exhibit photorefractive effects over the entire visible spectrum¹². The crystal was grown at the Ferroelectric Materials Department at the Rockwell International Science Center, in Thousand Oaks, California and was obtained through the U.S. Army Night Vision and Electro-Optics Laboratory in Ft. Belvoir, VA.

5. Measurable Consequences of the Photorefractive Effect

5.1) Beam Fanning. Transmitting a single incident beam, as from a laser, through a photorefractive crystal causes light to be scattered off defects and impurities that can combine with the main beam to produce standing waves.¹² The single beam enters the crystal and initially exits the crystal without change. Over time, the mobile charges of the crystal respond to the interference maxima and minima that are created in the standing wave patterns and set up photorefractive gratings. Because the impurities are not uniform in the crystal, the gratings written in this manner are random and set up a "fan" of scattered light to one side of the incident beam. This phenomenon is called beam fanning,^{1,11} and is shown in Figure 8.

Beam Fanning.

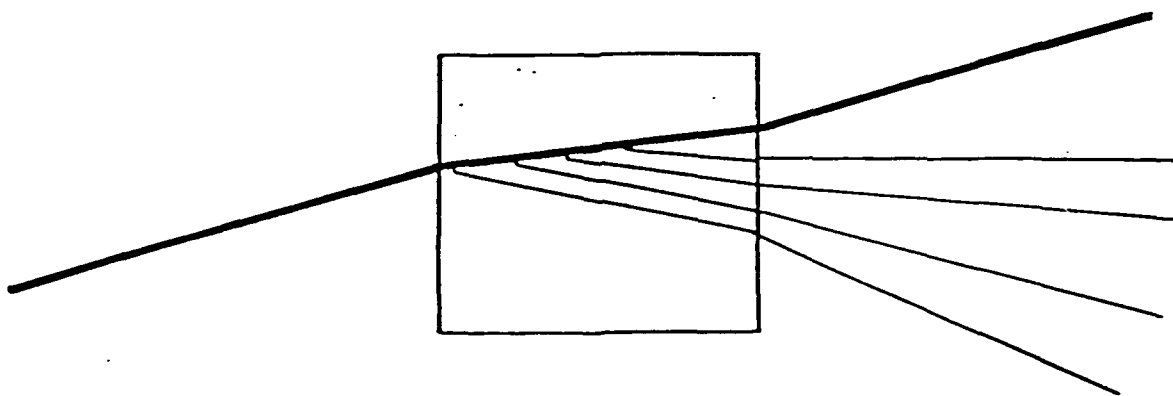


Figure 8.

The direction of the beam fan is dependent on the sign of the mobile charges in the material and the resulting direction of the relative

phase shift between the light intensity and the refractive index grating as discussed earlier.^{1,10}

The time for the beam fanning response varies from less than a second to minutes, and gives a measure of a material's ability to respond in a photorefractive way.

5.2) Optical Phase Conjugation. Photorefractive materials provide a means to produce optical phase conjugation. Optical phase conjugation is most easily described through the differences between a conventional mirror and a phase conjugate mirror. A conventional mirror with light incident on it will reflect that light such that the angle of incidence equals the angle of reflection and the normal component of the wave vector of the incident light is reversed in sign. A phase conjugate mirror, as shown in Figure 9, reverses the direction of the incident wave vector, as well as the phase of the incident light.

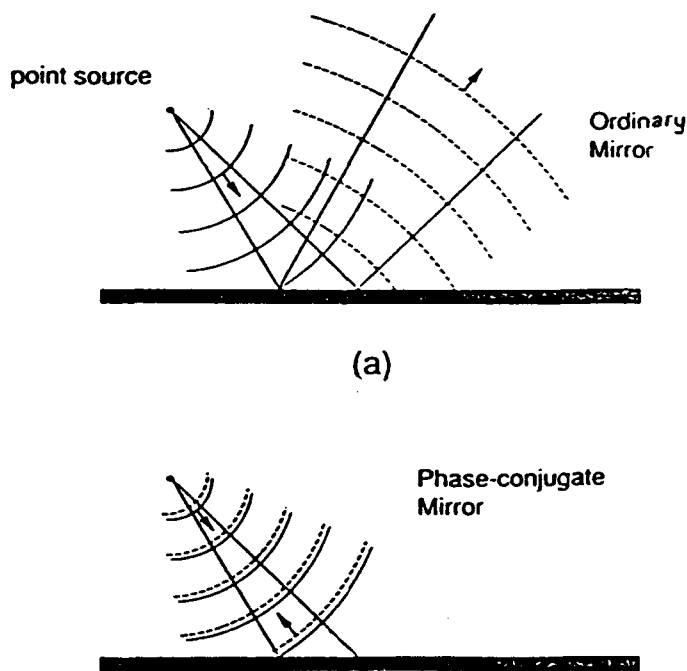


Figure 9. Ordinary/ Phase Conjugate Mirror Comparison

from Reference 11

For example, the electric field for an incident wave can be represented by

$$\mathbf{E}(\mathbf{r}) = \mathbf{E}_0(\mathbf{r})e^{i(\omega t - \mathbf{k} \cdot \mathbf{r})}, \quad (11)$$

where

$$\mathbf{E}_0(\mathbf{r}) = A_0(x,y)e^{i\phi(x,y)}. \quad (12)$$

The phase conjugate of the wave is

$$\mathbf{E}^*(\mathbf{r}) = \mathbf{E}_0^*(\mathbf{r})e^{i(\omega t + \mathbf{k} \cdot \mathbf{r})}, \quad (13)$$

where

$$\mathbf{E}_0^*(\mathbf{r}) = A_0(x,y)e^{-i\phi(x,y)}. \quad (14)$$

$A_0(x,y)$ and $\phi(x,y)$ are real-valued functions, ω is the angular frequency and \mathbf{k} is the wavenumber. In essence, the resulting

electromagnetic light is a time-reversed replica of the incident wave because only the spatial part of the wave has been conjugated, making it identical to the incident wave at every point in space, but traveling in the opposite direction.^{11,14,15}

Producing phase conjugation experimentally is a well-investigated area¹⁰ and two ways of producing phase conjugate waves will be examined here: holography and the photorefractive effect. Both of these examples rely on the non-linear properties of the materials, i.e., changes in the material due to the incident light.

5.2.a. Holography. As shown in Figure 10., a holographic exposure can be created using a reference beam as it interferes with the object beam on some photographic film.¹¹

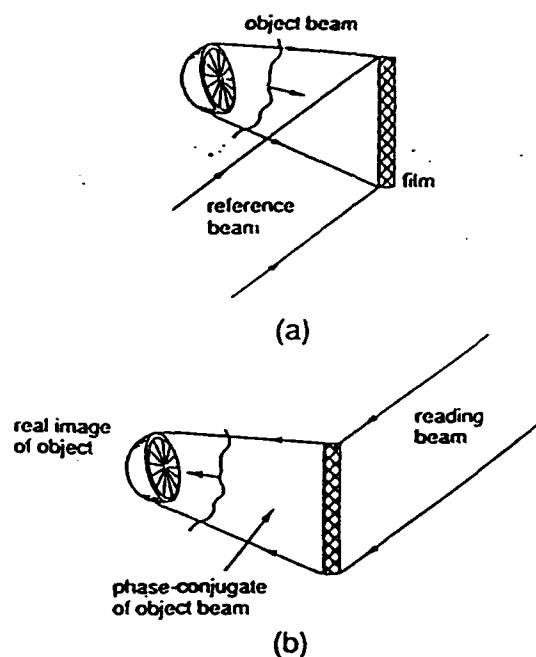


Figure 10. Two Steps of Holography (top to bottom) from Reference 11

After developing the film, the hologram can be "read" using a beam directed opposite to the original reference beam. This so-called read beam diffracts off the interference pattern stored on the exposed film, such that a real image of the original object is formed.¹¹

5.2.b. Four-Wave Mixing. Similar gratings can be formed in photorefractive materials. One way to form these gratings is called four-wave mixing which contains all the components of the holographic method, but is able to create the gratings and then respond to them in real-time. The advantage of this method over holography is that the wait to develop the film is no longer necessary. The four beams are shown in Figure 11 and it is important again to note that the pump beams, which play the roles of the reading and reference beams from the previously mentioned holography case, are identical except that they are oppositely directed.¹⁰

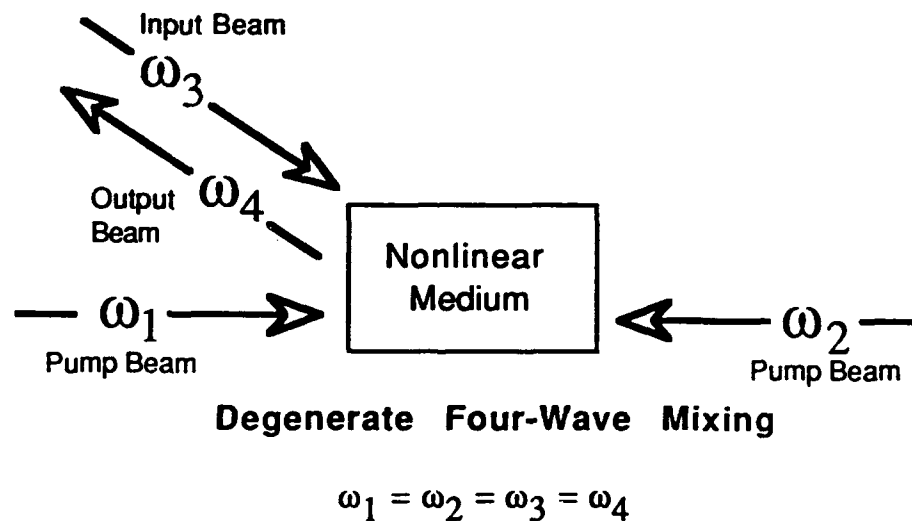


Figure 11

While an improvement over the holographic method, the four-wave mixing has the difficulty that the two external pumping beams must be perfectly aligned for efficient production of a phase conjugate wave. This problem is significantly reduced in the self-pumped phase conjugator.^{11,13}

5.2.c. Self-Pumped Phase Conjugation. Because of the high refractive index of photorefractive crystals relative to the air just outside, light from the beam fan directed near the corner of the crystal can easily be totally internally reflected, if correctly positioned.¹¹ This total internal reflection creates an interference pattern with the original input beam. The grating that is formed can produce a phase conjugate mirror, and is thus called self-pumping. Self-pumping of the photorefractive materials has some advantages over other techniques in the production of phase conjugate waves. Because it is self-contained, tedious alignment of reading and reference beams is avoided. Known also as a "cat" conjugator, the physical mechanisms that allow for self-pumped phase conjugation are not yet fully explained. As shown in Figure 12., the photorefractive effect "fans" light into the corner of the crystal and sets up the necessary reference and reading beams for phase conjugation in the circled regions, through total internal reflections at the corner of the crystal^{11,13}.

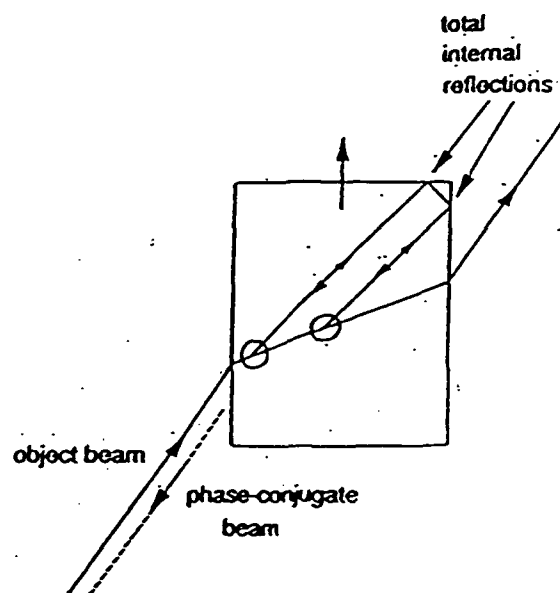


Figure 12. Self-Pumped Phase Conjugation from Reference 11

The ability of the phase conjugate signal to correct for aberrations and distortions as an optical beam is double-passed through a poor-quality optical system has several potentially useful applications.¹⁵ Targeting is one example of the benefit of exactly retracing the incident light's path back from the phase conjugate mirror. As shown in Figure 13, seed light incident on a target from an illuminator could be reflected into a laser amplifier.

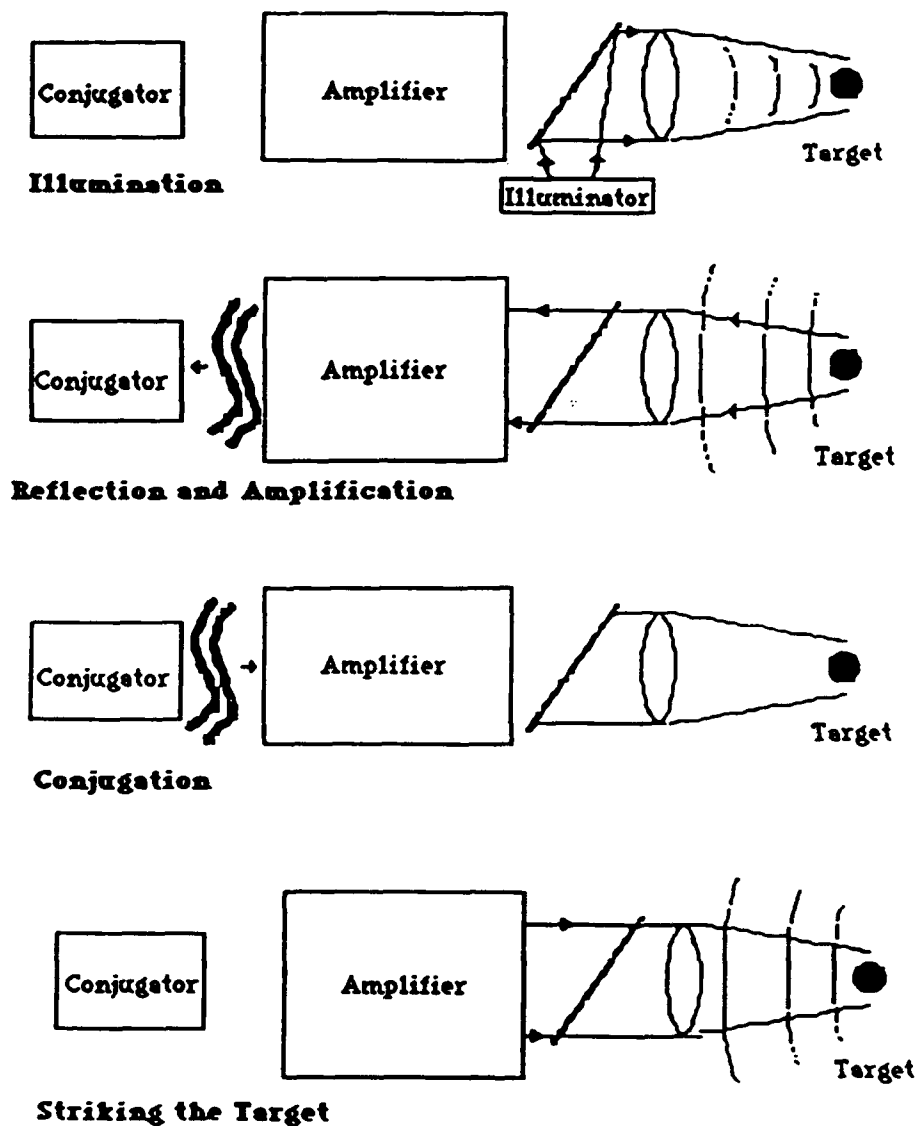


Figure 13. Targeting Application Steps (top to bottom)

The phase conjugate mirror would return the amplified light along the exact same path as the seed light and strike the target with much greater intensity. One such target could be a nuclear pellet. Laser fusion would require several lasers simultaneously striking a small, pellet target. Several pairs of amplifiers and phase conjugate mirrors could be arranged around the nuclear target pellet to accomplish that task effectively.^{14,15}

6. Experimental Setup

6.1) Picosecond Laser System. For this investigation of the photorefractive effect, the picosecond laser system in Michelson Lab B-7 was used to produce the ultrashort optical pulses needed. The system consists of an argon ion laser synchronously mode-locked to a wavelength-tuneable dye laser.

The mode-locker for the system is a piezoelectric transducer attached to a prism that is at one end of the ion laser beamline, just in front of its high reflecting mirror. The transducer is driven by an electrical signal at a frequency between 40-42 MHz and converts the electrical energy into acoustic energy, causing a periodic change in the refractive index of the prism. The resonant, standing acoustic wave in the prism functions effectively as a shutter, only allowing the light to be properly aligned (for lasing) on the mirror twice during each cycle of the standing acoustic wave. The cavity length and mode-locker frequency are matched so that the packet of light that is at the shutter when it is open, is all the light that is allowed to lase, so that the mode-locked laser can be considered two mirrors with an optical pulse bouncing between them. The pulses produced by the ion laser are approximately 120 picoseconds in length and at a wavelength of 514.5 nanometers. These pulses are used to stimulate the dye laser.

The dye, a combination of ethylene glycol and rhodamine 6G, is sprayed in a very thin stream upon which the incoming pulses from the argon laser are focused. The molecules of the dye reach excited states after being hit by an argon pulse and have a very large cross-

section for stimulated emission. When a pulse inside the dye laser cavity encounters the excited dye molecules they are quickly quenched due to their high cross-section for stimulated emission and their relative proximity in the thin dye stream. The amplified dye pulse is consequently much shorter than the exciting ion laser pulse. The cavity lengths are adjusted so that the arrival of the pulses from the ion and dye lasers at the dye stream is synchronized. The resulting pulses are as short as two picoseconds in length with a wavelength tunable between 570 and 660 nanometers.

With ultrashort pulses from the above source configuration, the beam was split with a beamsplitter in order to monitor the source pulses with the autocorrelator while investigating the photorefractive effect.

6.2) Beam Fanning. Beam fanning, described earlier in section 5.1, was measured using the lasers described above. The set-up of the experiment is shown in Figure 14.

Beam Fanning Setup

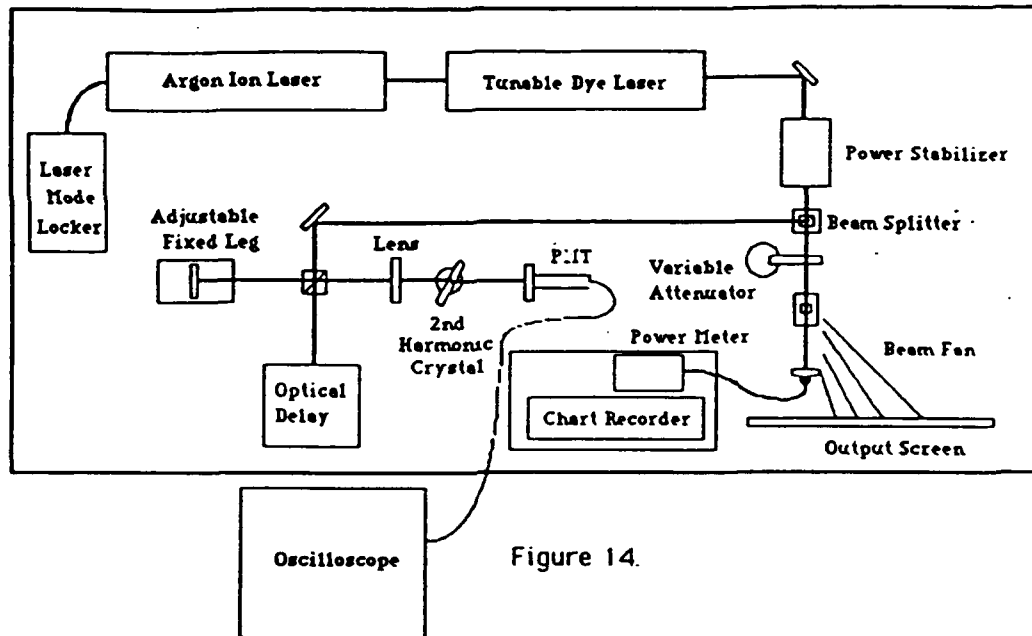


Figure 14.

The data was taken using the chart recorder to monitor the power output of the incident beam as it exited the crystal. A trace recorded by the chart recorder is shown in Figure 15. The fan time is taken as the time for the power output to decrease by a factor of $1/e$ relative to the difference between the initial and final throughput power from the crystal. The fan strength percent is the percentage of the initial throughput power that is fanned away from the detector and is computed with the expression:

$$\text{Fan Strength (\%)} = (P_0 - P_f) / P_0 \times 100\%, \quad (14)$$

where P_0 and P_f represent the initial and final power throughput from the crystal, respectively.

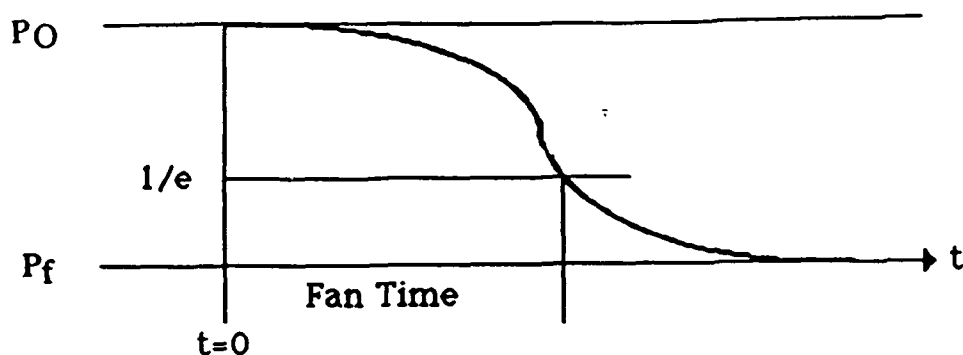


Figure 15. Beam Fanning Chart Recorder Trace

Three major sets of data were taken to record fan times of continuous wave and pulsed inputs at a wavelength of 592

Data Set #1

In the first set of data, the mode-locker was at a frequency of 41.1685 MHz, and the output on the autocorrelator was stable. The laser stabilizer was not being used, and there were slight instabilities in the output power.

Table 1. Data from 13 picosecond pulse

Initial Power (mW)	Fan Time (sec)	Fan Strength (%)
18.8	15.9	16.1
18.9	17.8	14.5
18.0	19.7	14.8
18.5	19.7	15.8
18.8	20.6	15.4
10.2	25.3	16.1
10.9	27.2	13.2
9.8	32.8	10.9
10.0	32.8	17.0
9.9	34.7	14.8
4.6	60.0	14.0
4.6	67.5	15.0
4.6	69.4	15.1
4.6	70.3	17.2
4.4	73.0	13.6
2.3	128.4	13.5
2.4	146.3	19.1

Table 2. Data from 4 picosecond pulse

Initial Power (mW)	Fan Time (sec)	Fan Strength (%)
18.1	20.6	10.0
19.5	22.5	11.8
10.0	33.8	10.0
10.3	37.5	10.9
5.0	58.0	10.1
5.0	62.8	9.9
2.5	128.0	11.3

Table 3. Data from CW laser

Initial Power (mW)	Fan Time (sec)	Fan Strength (%)
78.7	11.25	11.7
79.2	11.25	12.0
43.9	16.9	12.6
43.7	18.8	12.6
19.2	41.25	12.9
18.8	45.0	15.0
10.5	56.3	12.7
10.7	56.3	11.8
4.9	103.1	11.9
5.1	106.9	11.5

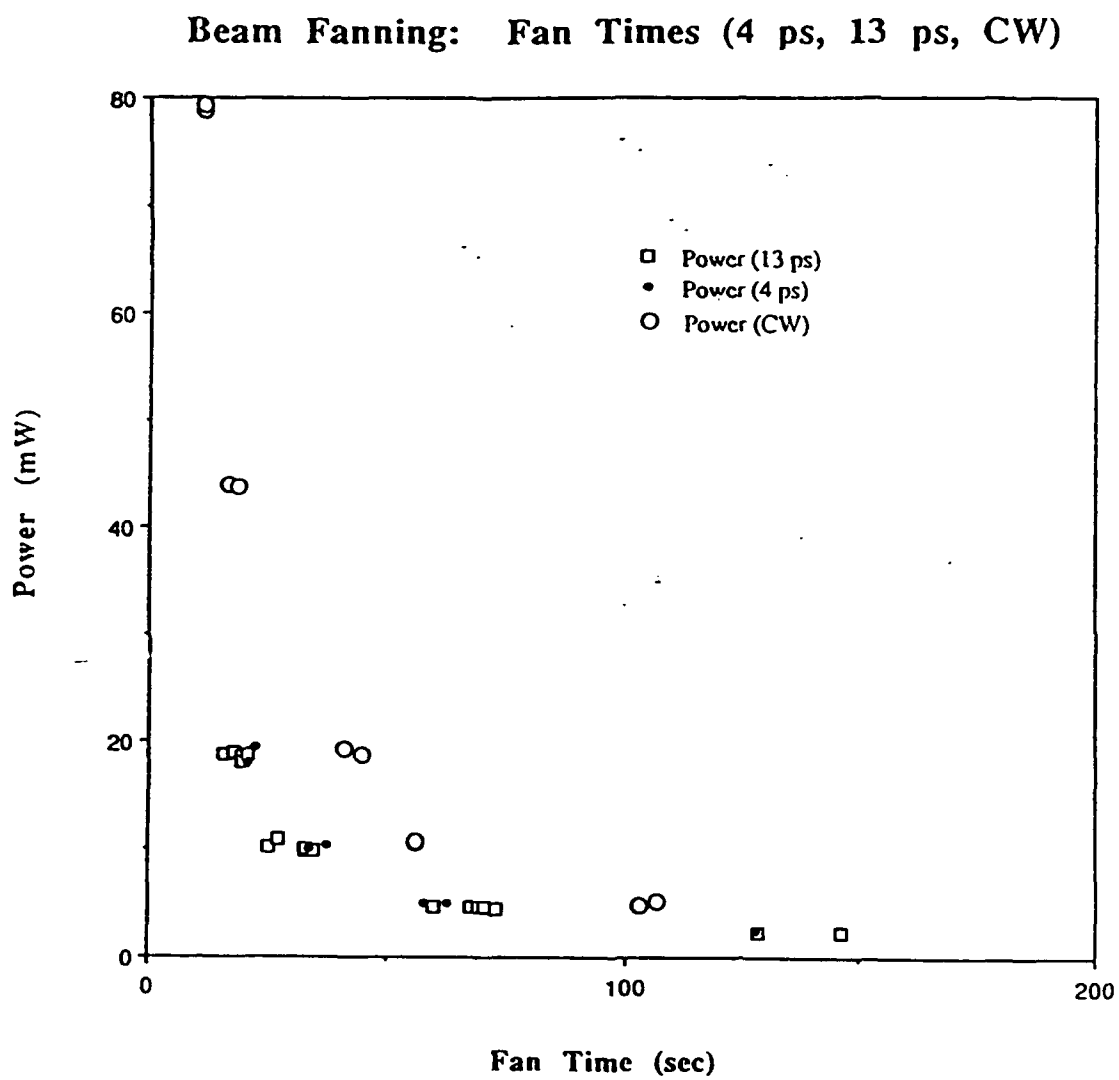


Figure 16.

Data Set #1 - Power vs. Grating Strength

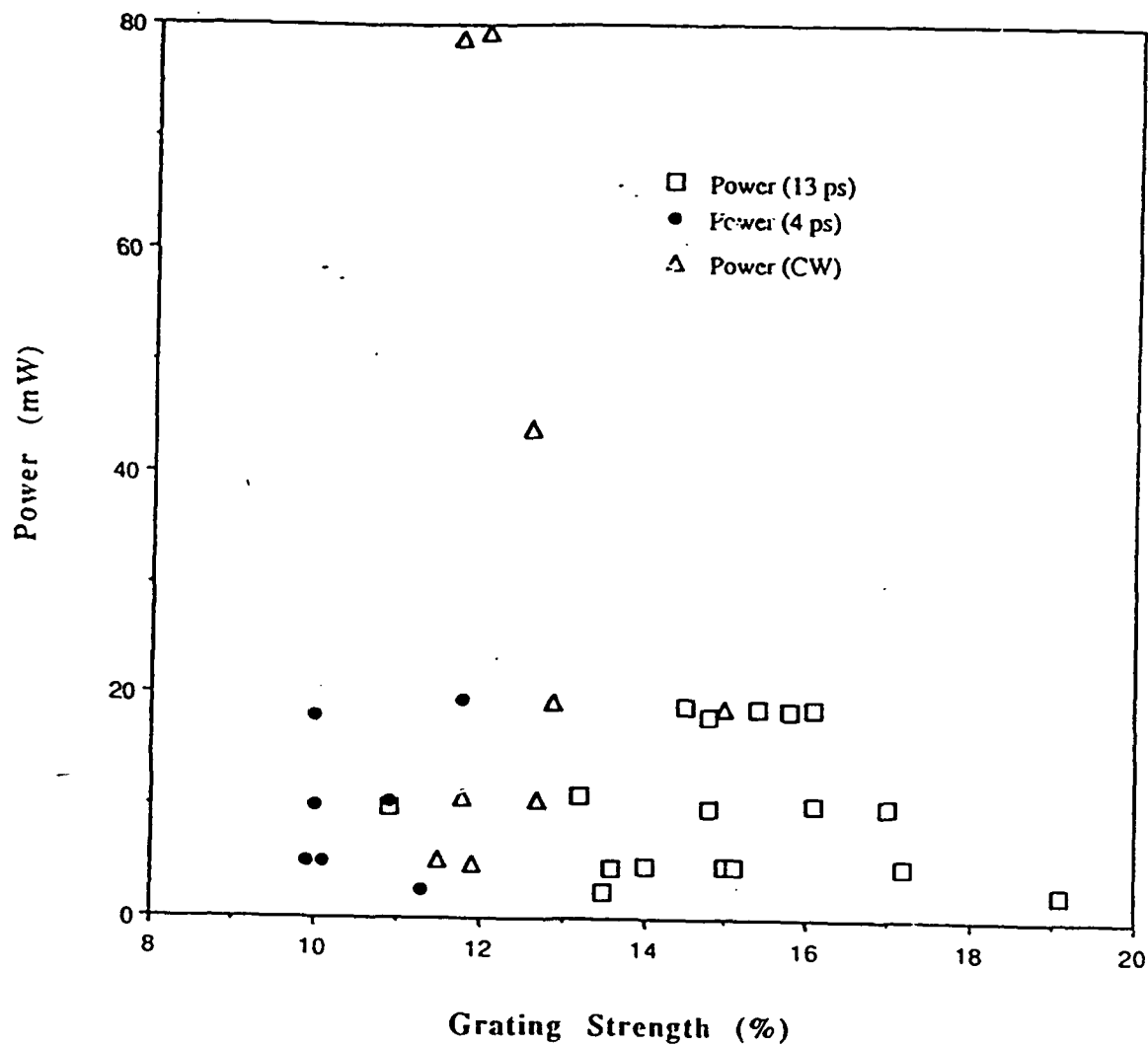


Figure 17.

Table 4.

Fan Strength	Mean	Standard Deviation
CW	12.5%	1.0%
13 ps	15.1%	1.8%
4 ps	10.6%	0.8%

The fan time results from Data Set #1 indicated that the CW fan times were significantly longer than the pulsed data, yet this was not confirmed by any subsequent data sets. When taking the CW data after the two pulsed sets, instead of turning off the power to the mode-locker completely and ensuring it did not interfere, it was simply reset. Subsequent results indicate that the failure to shut the mode-locker down most likely affected the operation of the laser in CW mode. The grating strength graph in Figure 17. shows the CW points flanked closely on either side by the pulsed data, and the difference is insignificant.

Data Set #2

In the second data set, the mode-locker was set at 41.1705 MHz. The pulses were significantly noisier at the higher frequency, and were more difficult to take readings from, especially the 6.5 ps pulse. The mode-locker was completely shut off after taking the pulsed data, and therefore was not able to interfere with the laser as it did in data set #1,

Table 5. Data from 6.5 picosecond pulse

Initial Power (mW)	Fan Time (sec)	Fan Strength (%)
12.37	10.31	23.1
10.68	12.2	20.1
4.93	36.56	22.3
4.62	39.38	20.3
2.55	59.06	20.8
2.85	65.16	21.8
2.48	66.56	20.2
2.7	75.0	22.2

Table 6. Data from 5 picosecond pulse

Initial Power (mW)	Fan Time (sec)	Fan Strength (%)
1.859	12.19	16.6
1.684	13.13	
1.863	13.13	16.4
1.105	17.81	16.9
1.08	20.63	17.2
1.117	21.09	15.6
5.35	36.56	15.5
5.48	41.25	16.8
5.51	47.81	
2.53	62.34	15.8
2.43	73.12	18.1
2.57	73.59	18.3

Table 7. Data from CW laser

Initial Power (mW)	Fan Time (sec)	Fan Strength (%)
18.34	13.59	19.5
15.52	16.41	19.5
12.34	17.34	19.8
14.04	16.41	19.5
8.93	27.19	18.6
10.31	23.91	19.4
6.62	35.16	19.2
4.79	52.97	19.6
2.95	103.59	19.7
7.2	30.47	19.
2.89	79.69	19.4
1.51	121.41	19.9
14.31	15.94	19.2
13.8	17.34	20.1
23.7	11.25	20.7
7.75	29.06	18.1

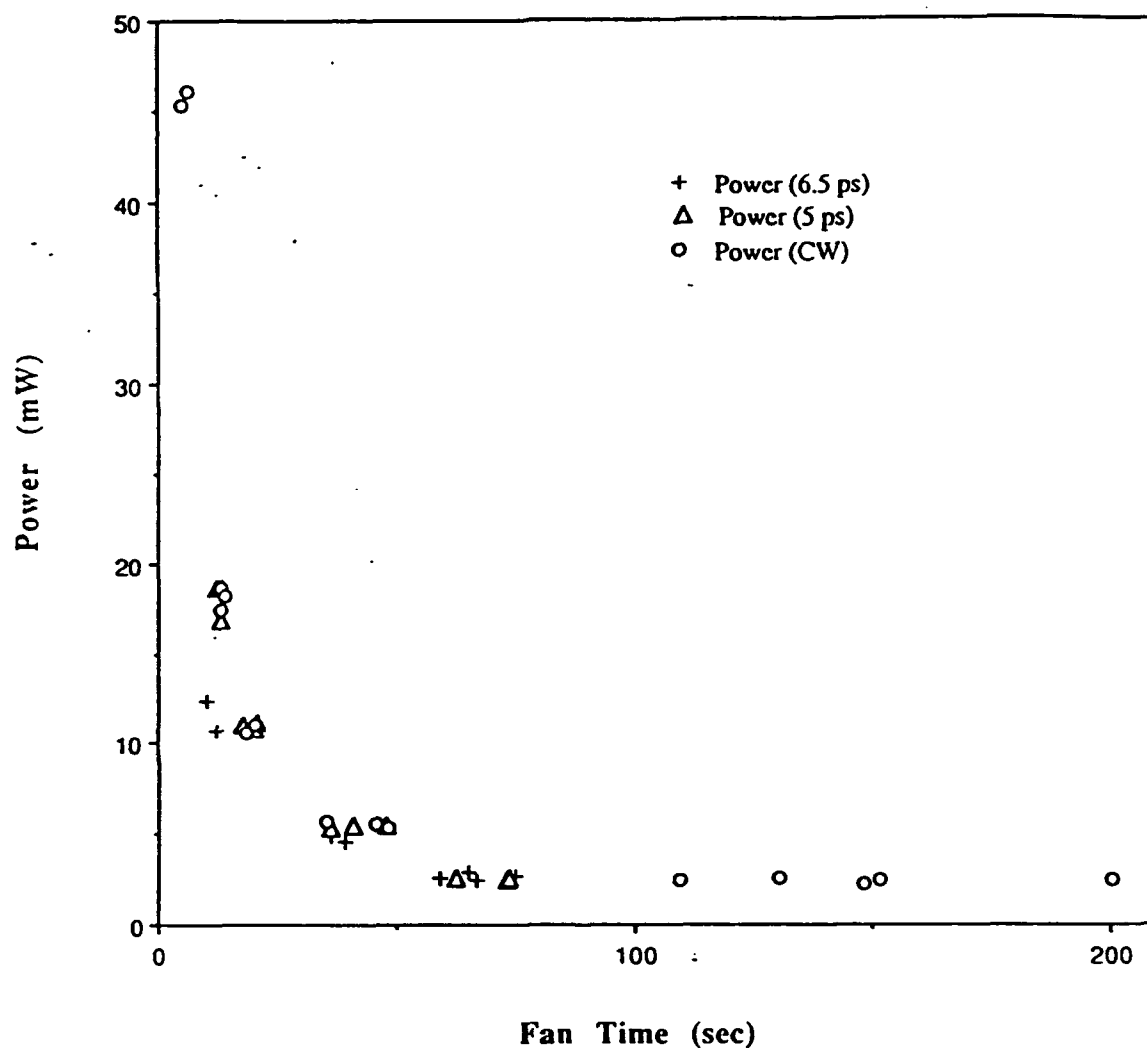
Data Set#2 - Power vs. Fan Time

Figure 18.

Data Set#2 - Power vs. Grating Strength

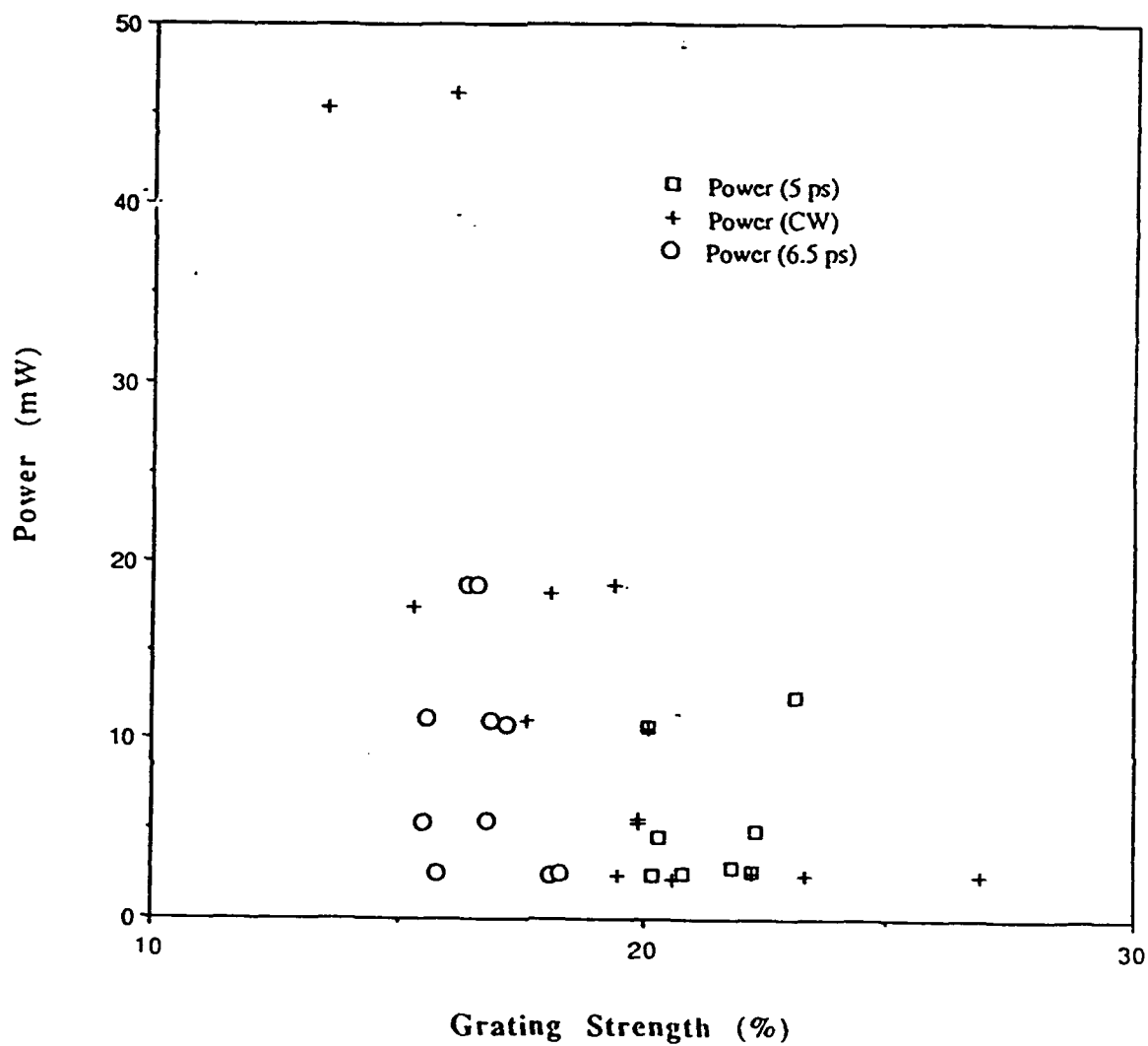


Figure 19.

Table 8.

<u>Fan Strength</u>	<u>Mean</u>	<u>Standard Deviation</u>
CW	19.5%	0.6%
6.5 ps	21.4%	.11%
5 ps	16.7%	1.0%

This data set indicates that there is no significant difference between the grating strength of the CW case and that of the pulsed case. A difference is seen between the pulsed and CW low power fan times, but that difference is refuted in Data Set #3. The low power readings of Data Set #2 fluctuated more than those of Data Set #3, a difference accounted for by laser power fluctuations that were later removed by using a laser power stabilizer.

Data Set #3

The third set of data was taken using the laser power stabilizer. The mode-locker was set at 40.7795 MHz, and the pulses were very clean. The readings were the least noisy of the three sets.

Table 9. Data from CW laser

Initial Power (mW)	Fan Time (sec)	Fan Strength (%)
23.7	11.25	20.7
18.34	13.59	19.5
15.52	16.41	19.5
14.31	15.94	19.2
14.04	16.41	19.5
13.80	17.34	20.1
12.34	17.34	19.8
10.31	23.91	19.4
8.93	27.19	18.6
7.75	29.06	18.1
7.20	30.47	19.0
6.62	35.16	19.2
4.79	52.97	19.6
2.95	103.59	19.7
2.89	79.69	19.4
1.51	121.41	19.9

Table 10. Data from 4 picosecond pulse

Initial Power (mW)	Fan Time (sec)	Fan Strength (%)
18.18	22.66	17.2
17.84	17.81	17.8
16.32	21.56	16.8
15.09	21.56	17.1
13.88	26.25	16.7
10.43	25.78	18.3
9.4	32.81	16.7
9.38	37.97	17.4
8.78	31.88	18.2
6.94	43.59	16.9
6.84	43.59	19.2
6.26	44.53	18.5
5.54	52.03	19.5
2.88	86.72	18.4
2.84	89.06	19.
2.47	163.59	16.2

Table 11. Data from 9 picosecond pulse

Initial Power (mW)	Fan Time (sec)	Fan Strength (%)
15.29	19.22	16.0
13.33	19.22	17.0
12.56	19.22	17.3
11.21	23.91	18.5
10.76	27.19	18.6
9.00	33.75	17.4
7.91	35.16	17.7
7.22	32.81	19.0
5.53	40.31	19.0
4.70	64.22	17.4
2.87	72.19	19.2
2.76	78.28	16.7
2.35	87.66	18.3
1.40	148.13	17.9

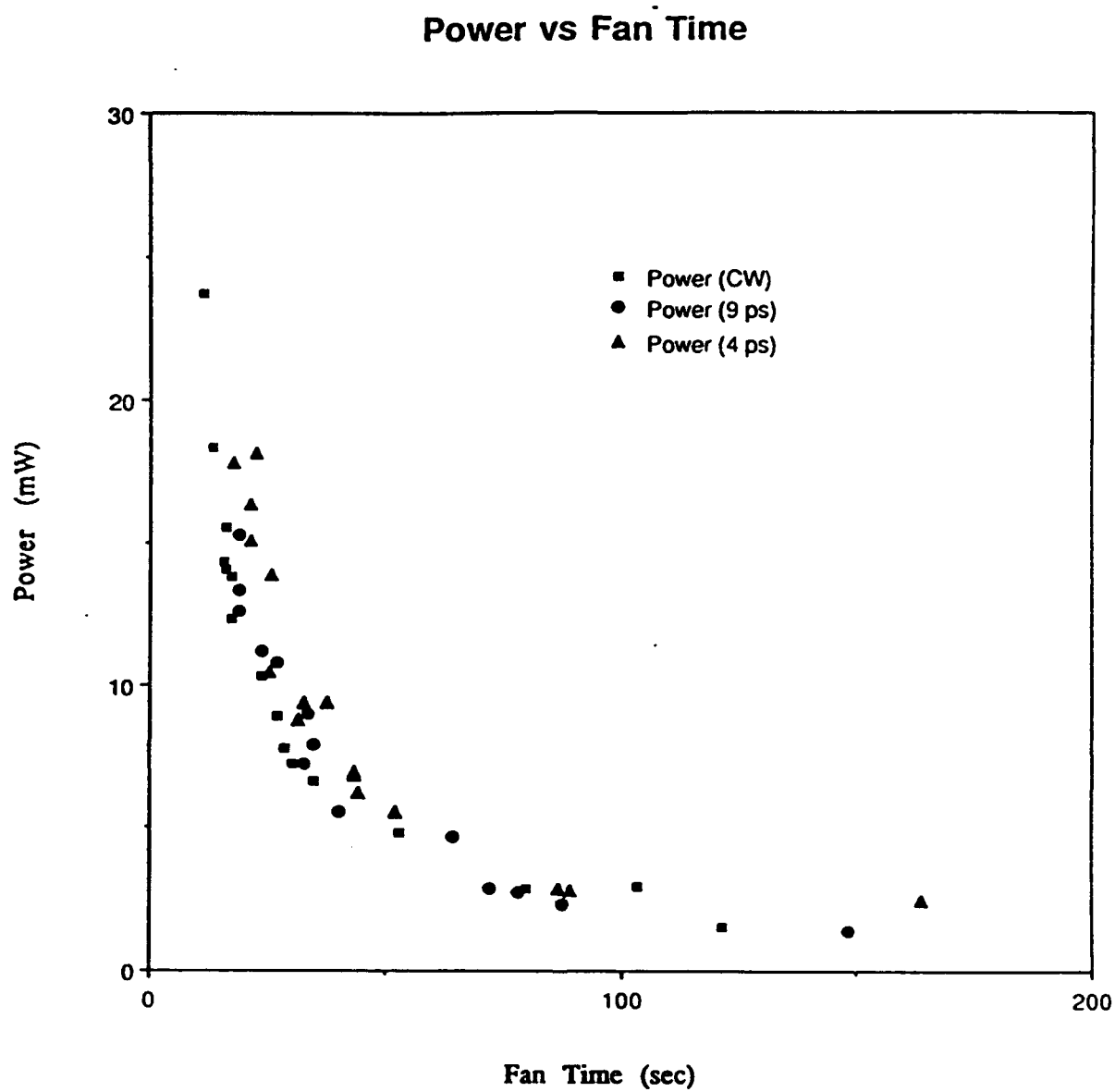


Figure 20.

Data Set #3 - Power vs. Grating Strength

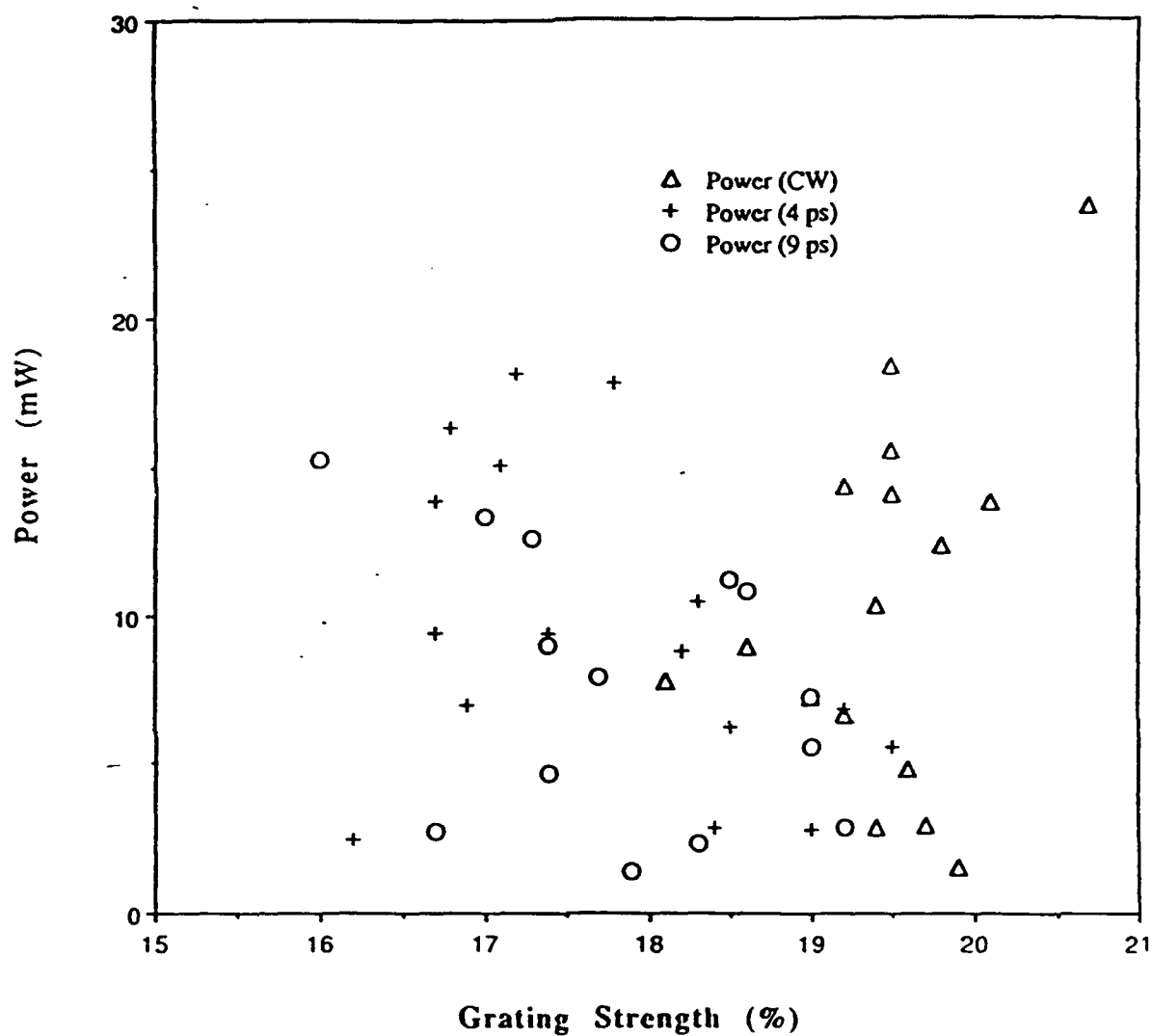


Figure 21.

Table 12

<u>Fan Strength</u>	<u>Mean</u>	<u>Standard Deviation</u>
CW	19.5%	0.6%
9 ps	17.9%	1.0%
4 ps	17.7%	1.0%

The results of Data Set #3 indicate that there is no significant difference between beam fanning data taken from CW input and pulsed input. The discrepancy between the pulsed and CW cases found in Data Set #1 we believe to be due to noise in the laser output. The shape of the Power vs Fan Time graph in Figure 20. appears to be hyperbolic in nature. An explanation for this is that the power multiplied by the time is a constant. This constant would correspond to the total energy or number of photons incident upon the crystal.

6.3) Self-Pumped Phase Conjugation. The set-up for the self-pumped phase conjugation portion of the experiment is shown in Figure 22.

Phase Conjugate Mirror Setup

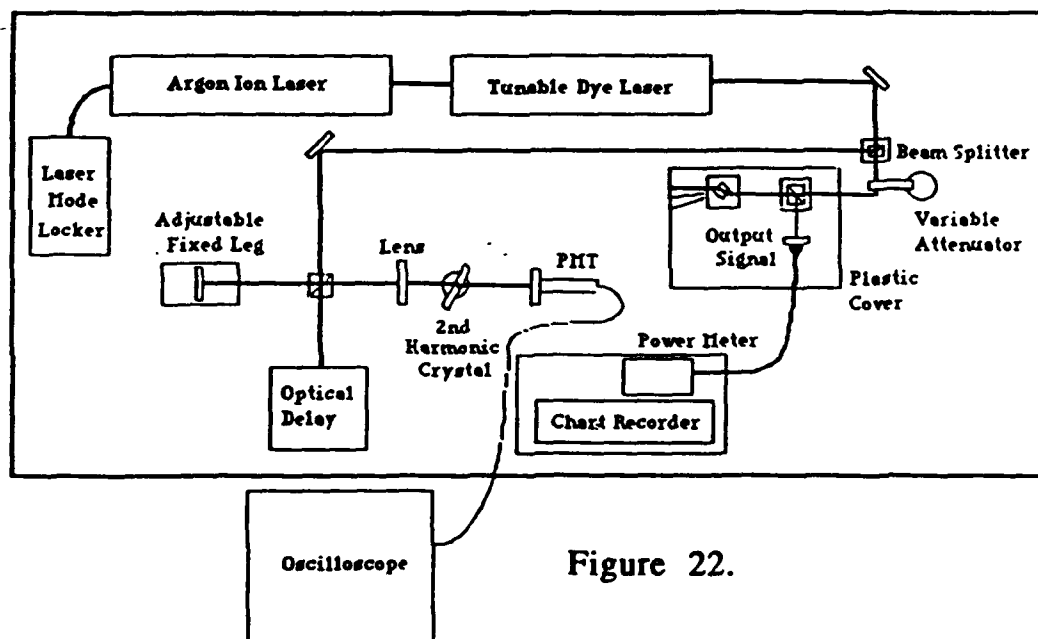


Figure 22.

The platform that held the crystal consisted of a turntable and translator so that different incident angles and positions on the crystal were able to be used. An anticipated result of this experiment was that picosecond pulses would not self-pump as a single train of pulses since light reflecting back from the corner of the crystal would probably not encounter any light with which to interfere.

This initial expectation was shown to be mistaken, and thus the first data set was to determine any differences between the grating formation time from CW or the picosecond pulses. The pulses used for this portion of the experiment were the longer, 9.5 ps pulses obtained by using the etalon because the shortest, 2.5 ps pulses would not self-pump at 45 degrees. All self-pumping measurements in this study were carried out using a laser wavelength of 566 nm.

**Table 13. Phase Conjugate Mirror (PCM) Data:
Angle of Incidence = 45 Degrees**

CW Input		9.5 ps Input	
Power	Grating Time	Power	Grating Time
91.6	44.06	33.9	122.0
50	70.31	27.1	150.0
30.2	138.	12.9	300.0
20.6	186.	6.17	605.4
10.7	270.	6.36	553.2
		40.7	92.34
		25.9	137.34
		12.9	286.88

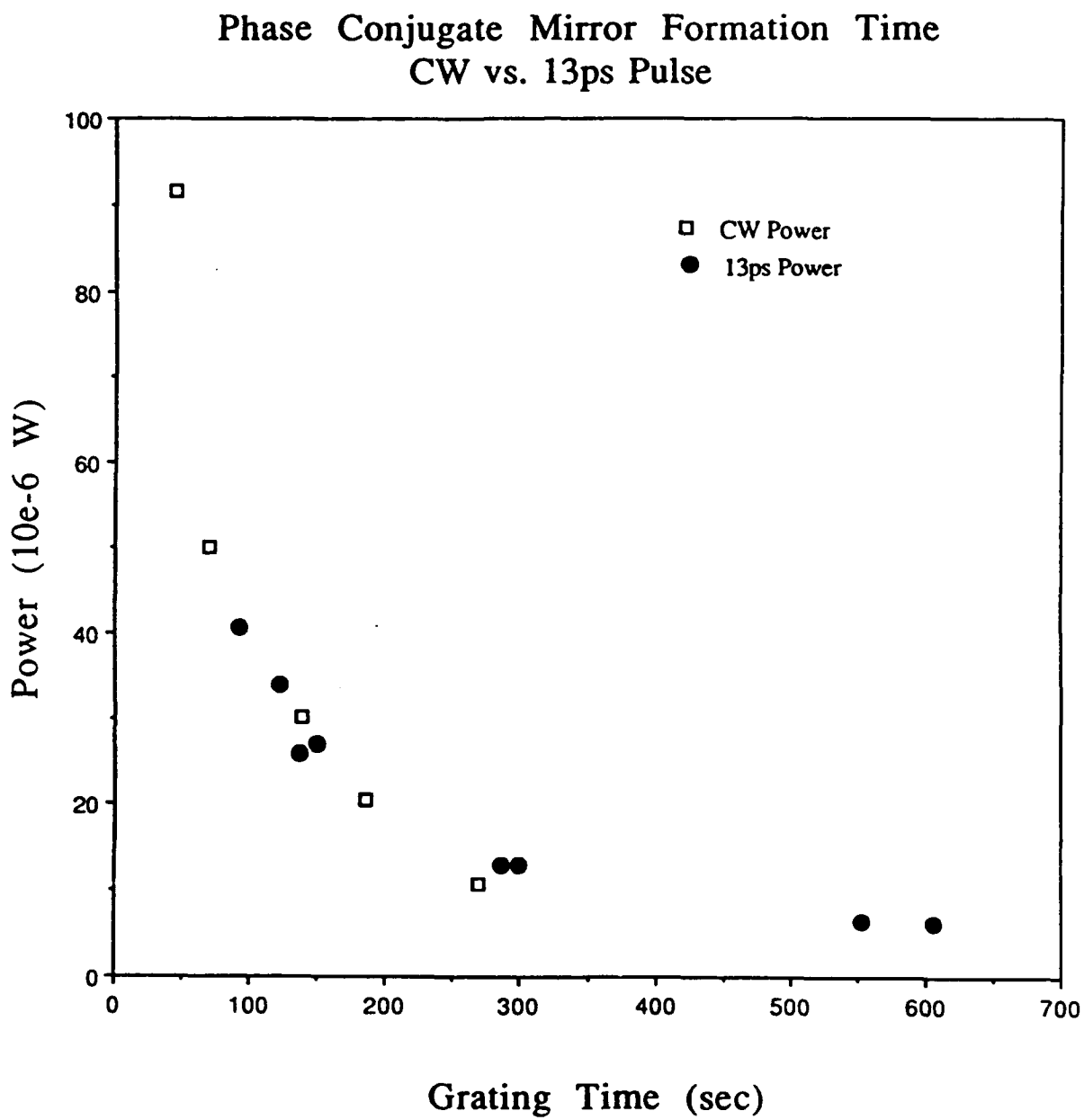


Figure 23.

Clearly, there is no significant difference between the grating formation times of the CW or pulsed cases, however, the self-pumped signals were extremely different.. The CW output was very noisy and sometimes contained periodic features, shown in Figure 24. There was no equivalent result from the pulsed input. One strong possibility that would potentially explain the unusual output is the feedback into the laser from the phase conjugate mirror. The pulsed output showed no indication of any similar feedback oscillations because the returning pulses were not precisely synchronized with the pulses present in the laser cavity. We can see the output in Figure 25.

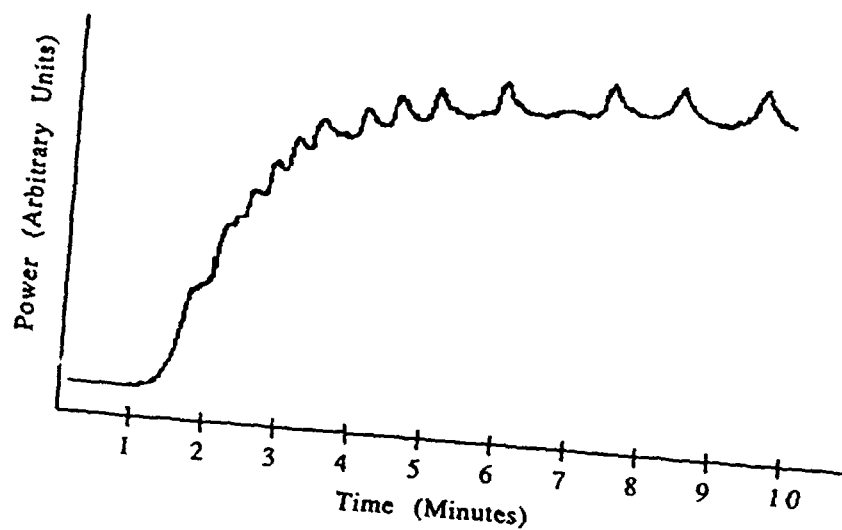
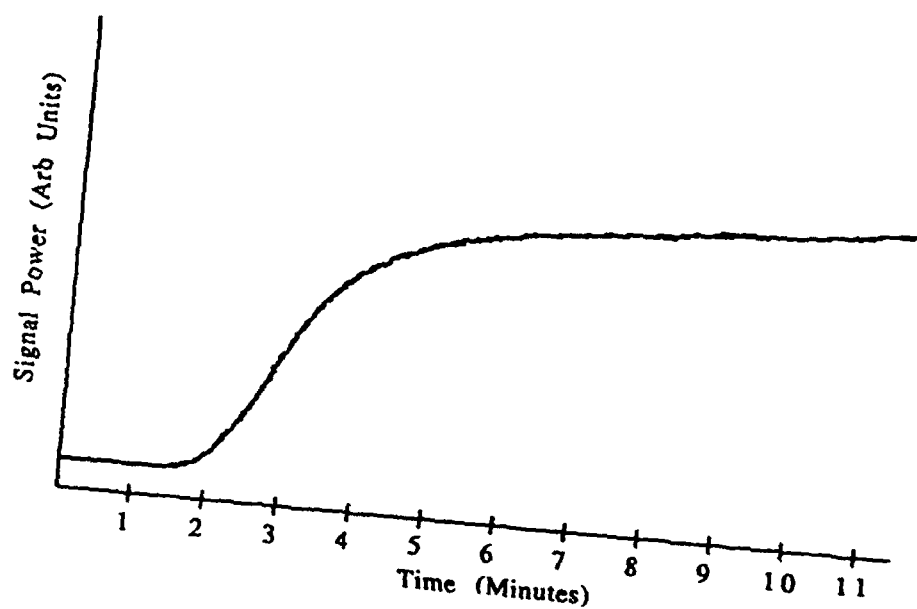


Figure 24. CW Phase Conjugate Signal



Rotating the crystal enabled the shortest pulses, 2.6 ps, to self-pump as the input angle increased.

Acceptance Angle Data

Table 14. 2.6 ps Pulse Input

Input Intensity (mW)	Signal Intensity (10^{-6} W)	Relative Reflectivity	Angle
61.0	7.08	0.116	54
91.0	7.88	.0866	53
77.5	6.38	.0823	52
77.5	6.38	.0823	52
77.5	5.17	.0667	51
77.5	5.66	.0730	50
77.5	5.66	.0730	49
77.5	5.29	.0683	47
77.5	2.95	.0381	45
77.5	20.3	0.262	55
77.5	24.6	0.317	60
77.5	36.9	0.476	65
77.5	42.4	0.547	70

Table 15.CW Input

Input Intensity (mW)	Signal Intensity (10^{-6} W)	Relative Reflectivity	Angle
77.5	320	4.13	20
77.5	413	5.33	30
77.5	453	5.85	40
77.5	420	5.42	50
77.5	403	5.20	55
77.5	592	7.64	60
77.5	635	8.19	65

Table 16. 9.5 ps Pulse Input

Input Intensity (mW)	Signal Intensity (10 ⁻⁶ W)	Relative Reflectivity	Angle
70	9.35	.1345	20
85	5.8	.0682	52.5
85	11.23	.1321	50
85	42	.4941	45
37	7.74	.2092	38
37	5.23	.1414	40
98	47.3	.4827	50
98	66	.6735	55
98	86	.8776	60
98	67	.6837	35
98	45.7	.4663	30

Two results seen from this data are the effect of the angle on the reflectivity of the phase conjugate mirror, and the relative reflectivity of the CW and pulsed inputs. These can be seen in the graphs of Figures 26 and 27. The rise in reflectivity for higher incidence angles is at least in part due to the fact that Brewster's angle, the angle at which the horizontally polarized input light is completely transmitted into the crystal, is 67° for BSKNN. Near Brewster's angle, the horizontally polarized light used to obtain self-pumping in this experiment, was more strongly transmitted into the crystal, resulting in higher power phase conjugate signals from both the pulsed and CW cases. Another factor may be that the fanned light bouncing around the corner of the crystal overlaps the incoming pulse more completely for large angles of incidence.

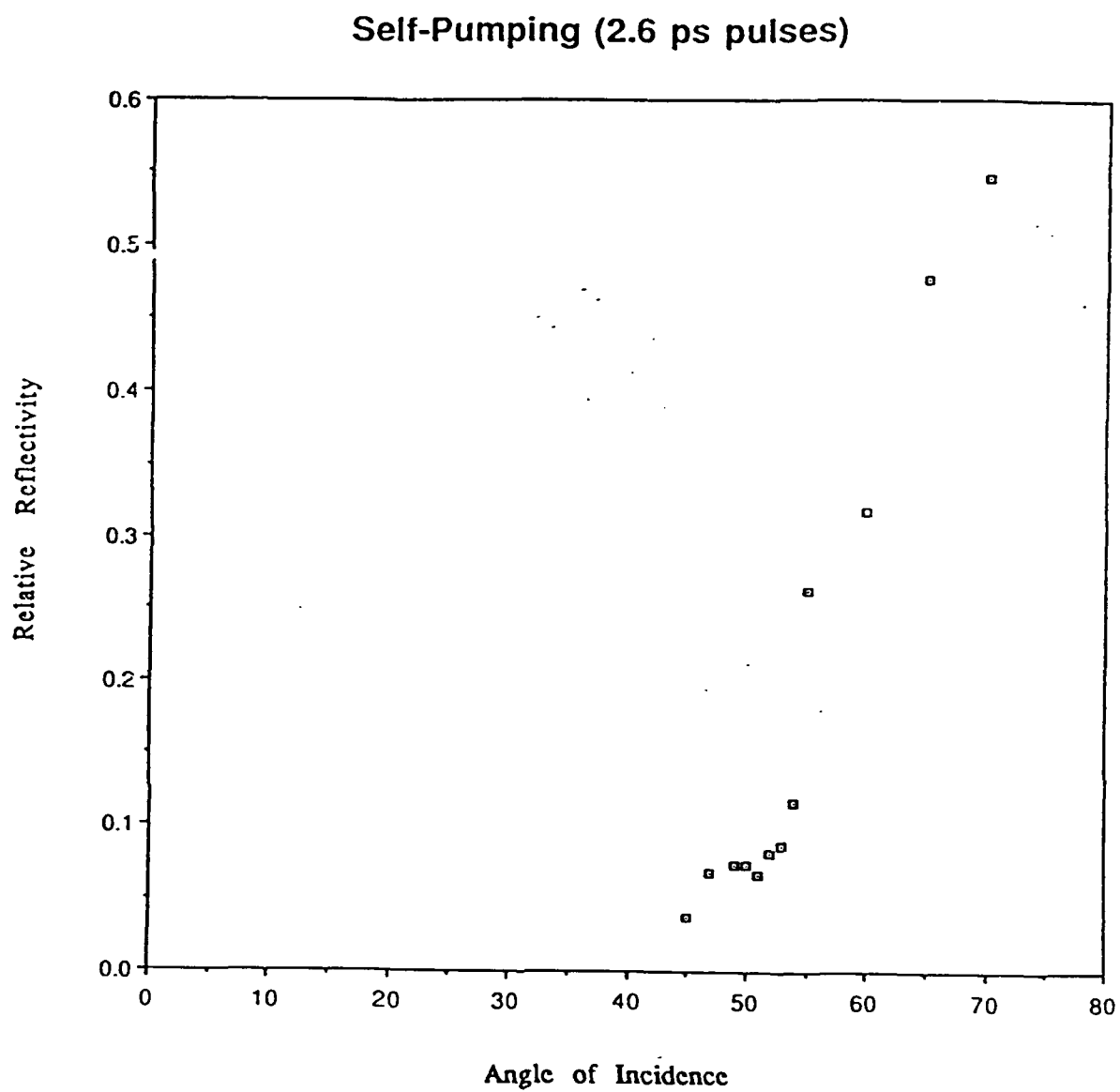


Figure 26.

Self-Pumping: CW/Pulse Comparison

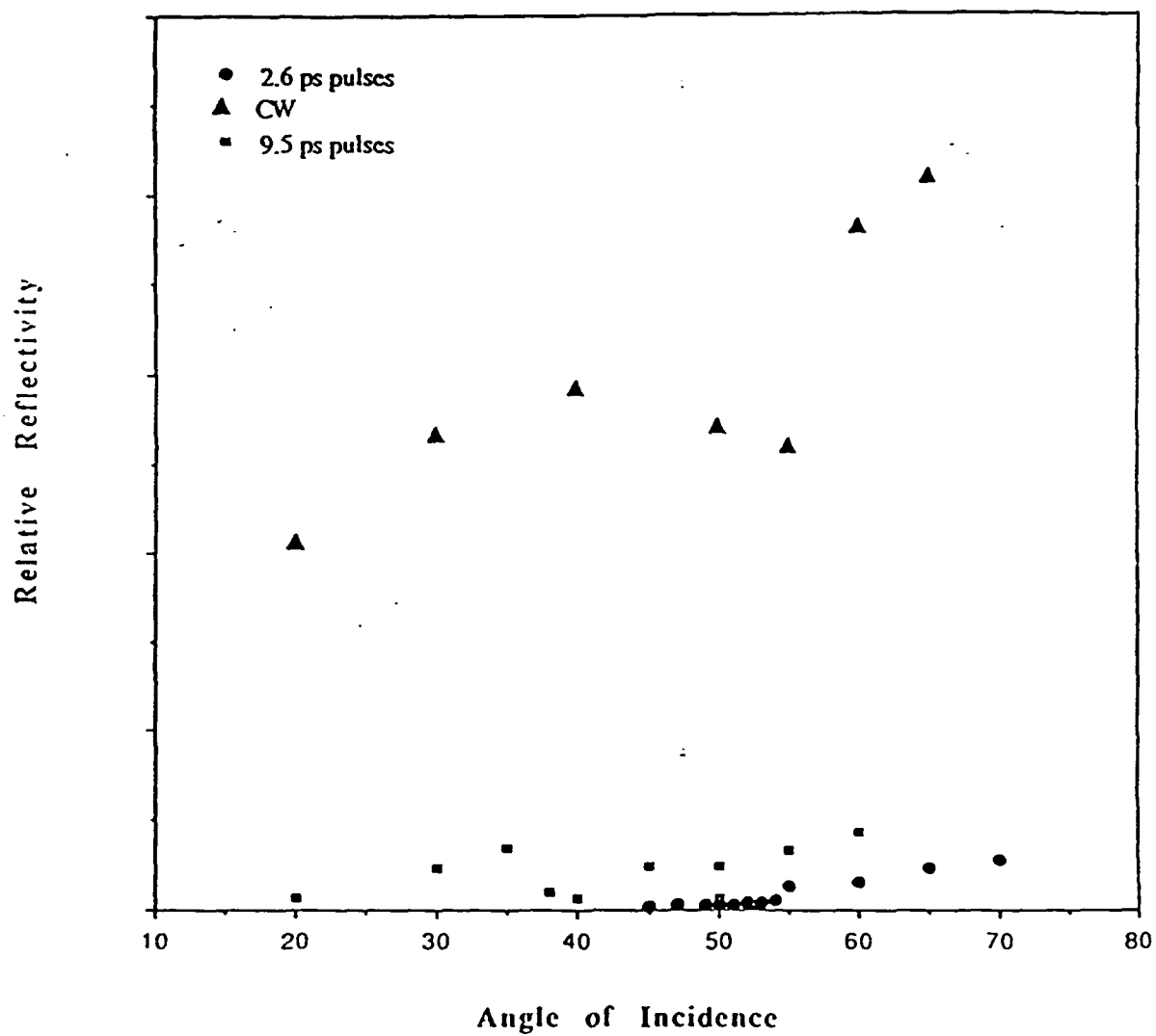


Figure 27.

With the 2.6 ps pulses as well as the 9.5 ps pulses, it was necessary to direct the beam almost into the corner of the crystal to obtain self-pumping. We can see the difference in CW and pulsed in Figure 28, that shows how pulses travel in the crystal. In air, a 3 ps pulse is only a millimeter long, and inside the crystal it is 2.4 times shorter (roughly 400 microns) so that the light energy in the pulsed case arrives in very thin slices.

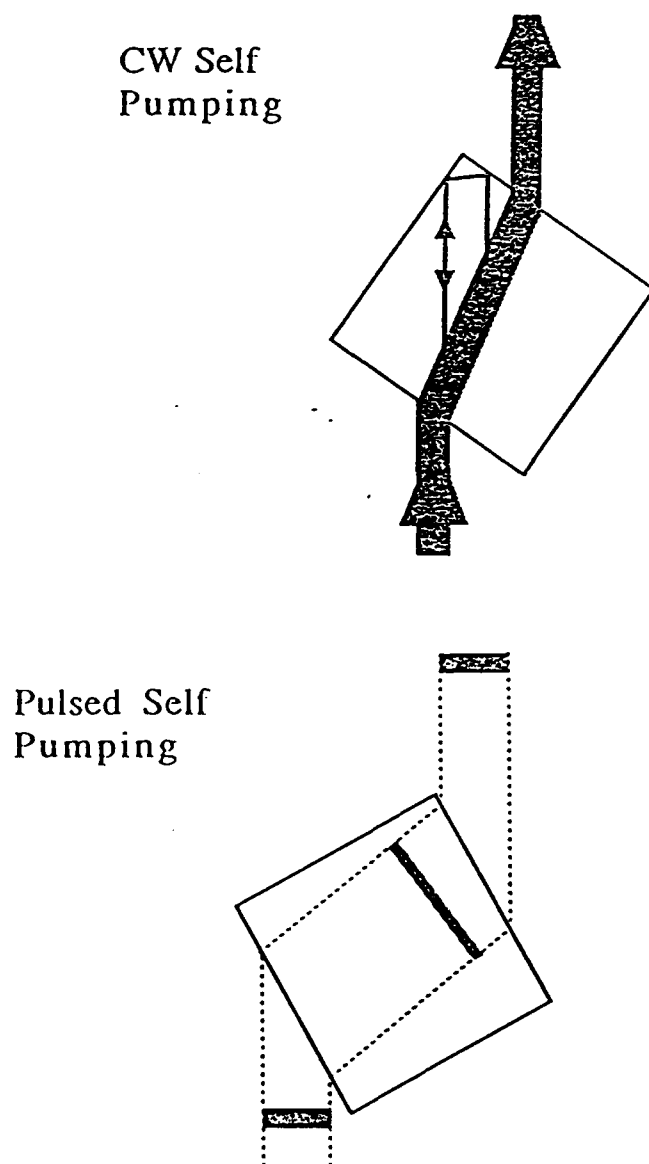


Figure 28. CW/ Pulsed Comparison of Light Interaction in BSKNN

7. Conclusions and New Directions

In this photorefractive experiment the objective was to investigate the difference between the photorefractive response of BSKNN to continuous wave or pulsed laser illumination. The optical autocorrelator constructed during the course of this experiment provides the ability to measure the pulse lengths, and to stabilize the synchronously mode-locked dye laser system. It will be a permanent addition to the Michelson B-7 laboratory.

The results of the beam fanning data indicated that the effect was dependent on the number of photons entering the crystal over a period of time. Therefore, using the same average power, CW or pulsed, produced fan times that were very similar.

The self-pumped phase conjugate signals showed distinct differences between the CW and pulsed cases. The CW inputs were noisy, occasionally had periodic features that were not seen in the pulsed signals, and were most likely the result of CW feedback into the laser cavity. The pulsed response did not show these features probably because the pulses returning back to the laser arrived out of step with the synchronous mode-locking and were quickly attenuated.

A test for checking phase conjugate feedback with pulses would be to change the distance between the laser and the crystal to see if, when the crystal is exactly a cavity length away, the noise would appear in the pulsed case. If it does then the noise is probably a feedback phenomena. If not, it is more likely a characteristic of the process taking place inside the crystal.

Another significant difference was that the CW phase conjugate signal was much stronger than the pulsed signal. Since the fanning times were the same, and the write times for grating formation were about the same, the ability of the light to move charges was the same in each case. Why is the phase conjugate reflectivity so different? The difference here is probably due to the difficulty of producing coherent overlap of light when the light is incident in the form of the very thin slices, as they are for ultra-short pulses inside the crystal. Further evidence of this is provided by the extreme sensitivity that was observed (but not quantified) with respect to placement of the

The results of this experiment have given more insight into the photorefractive effect. The response of the short pulses is consistent with previous models of self-pumped phase conjugation, as it was necessary to direct the beam near the corner so that the front end of the pulse could interact with its back end. The smoothness of the pulsed output signal makes it attractive for further investigation. Further studies will investigate possible enhancement of the self-pumped signal by sending two pulses into the crystal with a known time delay, so that the first will be totally internally reflected back to interact with the second pulse.

8. References

1. D. M. Pepper, J. Feinberg, and N. V. Kukhtarev, *Scientific American* 62, (October, 1990)
2. C. A. Burris, R. S. Tucker, and J. E. Bowers, *Electron. Lett.* 21, 262 (1985)
3. N. H. Schiller and R. R. Alfano, *Semiconductors probed by Ultrafast Laser Spectroscopy*, Vol. 2 (Academic Press, Orlando, FL, 1984), p. 151
4. S. R. Montgomery, D. O. Pederson, and G. J. Salamo, *Appl. Phys. Lett.* 49, 620 (1986)
5. J. A. Giordmaine, *Lasers and Light. Readings from Scientific American* 26, 295 (1964)
6. A. Yariv, *Optical Electronics*, 4th Ed., 275 (Holt, Rinehart, and Winston, New York, 1985)
7. P. A. Franken, A. E. Hill, C. W. Peters and G. Weinreich, *Phys. Rev. Lett.* 7, 118 (1961)
8. Spectra Physics Model 342A Ultra Stable Mode-Locking System Instruction Manual
9. Z. A. Yasa and N. M. Amer, *Opt. Comm.* 36, 406 (1981)
10. J. Feinburg, and K. R. MacDonald, *Opt. Lett.* 5, 156 (1988)
11. J. B. Norman, *Am. J. Phys.* 60 (3), 212 (1992)
12. S. R. Montgomery et al., *J. Opt. Soc. Am. B* (5), 1775 (1988)
13. J. Feinburg, *Opt. Lett.* 10, 486 (1982)
14. R. A. Fisher, *Optical Phase Conjugation*, 3 (Academic Press, New York, 1983)
15. C. R. Giuliano, *Physics Today*, 27, (April, 1981)

Appendix A: Equipment List

Spectra Physics Model 342A Ultrastable Mode Locking System

Spectra Physics Model 2040 High Power Argon Ion Laser

Spectra Physics Model 3500 Ultrashort Pulse Dye Laser

Cambridge Research & Instrumentation, Inc. Model LS200 Laser

Special Optics Model 8r-9012 Polarization Rotator

Jodon Engineering Associates VBA-200 Beam Splitter (Variable Attenuator)

Melles Griot Model 0385C005 .5" Beamsplitters

BSKNN Photorefractive Crystal

Femtochrome Research, Inc. Model FR-203 Optical Delay Generator

Inrad Model BB0-AG-2 (Beta Barium Borate) 2nd Harmonic

Generating Crystal (555-880 nm)

Oriel Model 12710 Filter

Newport Research Corporation Model LP-1-XYZ Photomultiplier Tube

Tektronix Model 7104 Oscilloscope

Newport Research Corporation Model 815 Power Meter

Varian Model G-2000 Chart Recorder